Journal of
Composites Science

MDPI

Article

The Use of Externally Bonded Fibre Reinforced Polymer Composites to Enhance the Seismic Resilience of Single Shear Walls: A Nonlinear Time History Assessment

Ali Abbaszadeh and Omar Chaallal *

Department of Construction Engineering, École de Technologie Supérieure, University of Quebec, Montreal, QC H3C 1K3, Canada; ali.abbaszadeh.1@ens.etsmtl.ca
* Correspondence: omar.chaallal@etsmtl.ca

Abstract: In medium- to high-rise buildings, single shear walls (SSWs) are often used to resist lateral force due to wind and earthquakes. They are designed to dissipate seismic energy mainly through plastic hinge zones at the base. However, they often display large post-earthquake deformations that can give rise to many economic and safety concerns within buildings. Hence, the primary objective of this research study is to minimize residual deformations in existing SSWs located in the Western and Eastern seismic zones of Canada, thereby enhancing their resilience and self-centering capacity. To that end, four SSWs of 20 and 15 stories, located in Vancouver and Montreal, were meticulously designed and detailed per the latest Canadian standards and codes. The study assessed the impact of three innovative strengthening schemes on the seismic response of these SSWs through 2D nonlinear time history (NLTH) analysis. All three strengthening schemes involved the application of Externally Bonded Fiber Reinforced Polymer (EB-FRP) to the shear walls. Accordingly, a total of 208 NLTH analyses were conducted to assess the effectiveness of all strengthening configurations. The findings unveiled that the most efficient technique for reducing residual drift in SSWs involved applying three layers of vertical FRP sheets to the extreme edges of the wall, full FRP wrapping the walls, and full FRP wrapping of the plastic hinge zone. Nevertheless, it is noteworthy that implementing these strengthening schemes may lead to an increase in bending moment and base shear force demands within the walls.

Keywords: single shear walls; permanent deformation; FRP sheets; self-centering; Canadian seismic zones; nonlinear time history analysis; resilience

Citation: Abbaszadeh, A.; Chaallal, O. The Use of Externally Bonded Fibre Reinforced Polymer Composites to Enhance the Seismic Resilience of Single Shear Walls: A Nonlinear Time History Assessment. *J. Compos. Sci.* **2024**, *8*, 229. https://doi.org/10.3390/jcs8060229

Academic Editors: Xiangfa Wu and Oksana Zholobko

Received: 18 April 2024
Revised: 11 June 2024
Accepted: 13 June 2024
Published: 17 June 2024

1. Introduction

Single shear walls (SSWs) are widely used in earthquake-resistant building designs because they are easy to build and cost-effective, and can add rigidity to high-rise buildings. These walls are subjected to different forces, such as axial forces from the gravity loads of the upper floors and shear force and bending moment resulting from the lateral forces applied to them. Based on the type of loading and response of tall SSWs, they can be modeled as cantilever beams, and their seismic response is governed by the bending moment. Modern design codes allow the shear walls to exhibit nonlinear behaviors, enabling them to undergo substantial distortions to absorb considerable amounts of energy effectively. The National Building Code of Canada (NBCC20) [1] mandates precise reinforcement detailing for shear walls with ductile properties to fulfill this role. Plastic hinges formed at the base of shear walls can cause permanent deformations in this Seismic Force Resisting System (SFRS).

Recent studies have focused on improving the seismic resilience of structures. In a study conducted by Bruneau and Reinhorn [2], they examined the resilience of structures to seismic events, focusing on both the social and structural dimensions of resilience. They defined structural seismic resilience as the capability of structures to experience significant deformation without major residual displacement. They established specific

thresholds for inter-story drift within nonlinear responses, which act as indicators of seismic resilience. The research also highlights how retrofitting affects the vulnerability and performance thresholds of buildings, pointing out the severe risks of structural collapses and failures without seismic retrofitting. One method to enhance resilience is by increasing the structure's strength and stiffness through high-resistance materials or larger dimensions, although this can be expensive and pose architectural challenges. Alternatively, structures can gain self-centering capabilities through either the inherent properties of the materials used or by incorporating attached self-centering systems [3].

Self-centering systems encompass two primary approaches. The first approach is categorized as (i) controlled rocking, which utilizes post-tensioned tendons for controlled motion [4]; (ii) uncontrolled rocking, which relies on the structure's self-weight for uncontrolled movement during seismic events [5]. In the second approach, specialized mechanical devices combining Shape Memory Alloys (SMAs) with energy dissipators can absorb and diffuse seismic energy [6,7]. Figure 1 illustrates the self-centering mechanisms that are frequently discussed in the seismic-related literature.

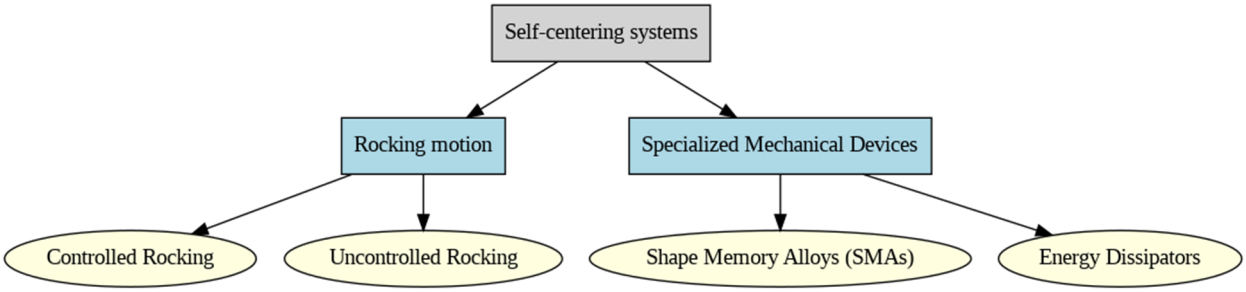

Figure 1. Self-centering mechanisms that are frequently discussed in seismic literature.

The seismic resilience of structures is also crucial in masonry structures. Some studies have explored resilience and collapse dynamics in masonry structures. Fortunato et al. (2017) [8] presented a new method to analyze masonry failures using a variational approach that accommodates discontinuities in crack formations. This method accurately predicts load-bearing capabilities and failure modes under various loads. Their work, demonstrated through computational simulations, offers essential insights into maintaining and preserving historical masonry buildings. Advanced methodologies for enhancing the seismic resilience of structures involve integrating contemporary high-performance materials, utilizing sophisticated analytical instruments to evaluate structural susceptibilities, and strategically applying retrofitting procedures to address shortcomings within pre-existing systems. To that end, the use of Fiber Reinforced Composites (FRP) features many advantages, encompassing an exceptional strength-to-weight ratio, inherent resistance to corrosion, easy incorporation within intricate architectural frameworks, and economic viability [3,9]. This technique consists of bonding FRP sheets onto the external surfaces of the shear walls, consequently bolstering their load-bearing capacity [10], ductility [11], flexural capacity [12], shear strength [13], and energy dissipation mechanisms [14]. El-Sokkary et al. [11] assessed the effectiveness of using Externally Bonded Fiber Reinforced Polymer (EB-FRP) in eight-story SSWs subjected to various seismic time histories representing the design spectrum of Montreal as a representative of the eastern Canadian seismic zone. The plain wall exhibited a second plastic hinge zone in the upper stories (sixth) due to the effect of higher vibration modes. EB-FRP strips were used to increase flexural and shear strength in the upper levels, while the wall base was confined to develop ductility. The strengthening scheme resulted in a significant reduction in wall rotation (up to 28%), a strain decrease in steel rebars, and an increase in demand for shear force and bending moment. Deng et al. [10] demonstrated that fully wrapping shear walls, especially at the base where plastic hinges are expected to form, can enhance damaged shear walls' load-carrying capacity and ductility. Cruze et al. [15] investigated the advantages of using horizontal EB-FRP sheets and showed a considerable increase in shear strength, ductility,

and energy dissipation with this strengthening configuration. They argued that implementing horizontal EB-FRP can improve their seismic behavior even if the wall does not require shear strengthening. El-Sokkary et al. [16] increased the flexural capacity of shear walls using 200 mm width EB-FRP strips on both sides of the wall. Horizontal FRP was used to follow the ductile seismic design philosophy and prevent brittle shear failure, resulting in an 80% improvement in flexural capacity. Other studies also confirmed the effectiveness of using vertical EB-FRP to improve the flexural strength of SSWs [14,17].

Some studies have investigated the impact of using EB-FRP on the energy dissipation capacity of shear walls [11,18]. The findings by Cruze et al. [15] indicated that increasing the number of FRP layers, especially those oriented both vertically and horizontally, significantly enhances the energy dissipation and ductility of RC shear walls. Also, including horizontal FRP reinforcement is crucial, as it prevents premature shear failures and maintains structural integrity even after initial FRP debonding. These insights highlight the importance of optimizing FRP layers' quantity and orientation to maximize the energy dissipation capacity and seismic resilience of RC shear walls.

Previous studies showed that deploying EB-FRP sheets amplifies the lateral resistance of shear walls against seismic forces and avoids the need for substantial structural reinforcement and reconstruction caused by severe seismic loadings, streamlining the overall upgrading process. However, no research study in the literature directly evaluates the decrease in the residual displacement of SSWs strengthened with EB-FRP sheets. A study on innovative methods to reduce residual displacement in coupled shear walls (CSWs) by Abbaszadeh and Chaallal [3] found that using fully wrapped FRP and vertical layers of EB-FRP can reduce inter-story drift, beam rotation, and residual inter-story drift in the walls located in Canadian seismic zones. In addition, various research studies have investigated alternative techniques for reducing residual deformation in shear walls, such as CFRP grids [19], hybrid CFRP grids–steel [20], and CFRP bars [21]. Nevertheless, there has been no emphasis on reducing residual displacement and increasing resilience and self-centering in pre-existing SSWs by employing EB-FRP sheets.

This has been the main impetus to investigate the effectiveness of different EB-FRP sheet configurations in reducing inter-story drift in existing SSWs in terms of pivotal seismic indicators encompassing residual inter-story drift, shear force, bending moment, and inter-story drift. Accordingly, a total of 208 nonlinear time history (NLTH) analyses via RUAUMOKO 2D software are utilized to thoroughly assess 20-story and 15-story SSWs located in the seismic zones of Vancouver and Montreal. The walls are subjected to different magnitude–distance ground motion scenarios corresponding to each city's uniform hazard spectrum (UHS). Various strategies are used to test the SSWs' behavior, encompassing an unstrengthen SSW and three SSWs strengthened with innovative EB-FRP configurations. The nonlinear response of the shear wall is determined by analyzing the mean value of all shear wall responses to the selected ground motions. Each wall in Vancouver was evaluated using 15 ground motions, while 11 ground motions were used for the walls located in Montreal. The analysis outcomes clearly illustrate the influence of the strengthening schemes on the assessed variables.

After the introduction, the study is explained through a series of focused sections. Section 2 begins our exploration by examining the design standards that govern the construction of ductile shear walls. Section 3 provides detailed insights into the architectural and seismic design specifics of the analyzed buildings. In Section 4, we delve into the strategic application of FRP composites to bolster the structural resilience of shear walls. Section 5 outlines the analytical methods employed to simulate the seismic response of these reinforced structures. Section 6 evaluates the impact of FRP reinforcements, focusing on their effectiveness in reducing residual displacement of shear walls. The paper concludes with Section 7, which highlights the most important discoveries.

2. Seismic Design of Ductile SSW According to Standards

According to CSA A23.3-19 [22], the factored shear force at the base of SSWs should be calculated using either the equivalent static force procedure or the dynamic analysis specified in NBCC20. The base shear force must be increased to account for flexural overstrength and the plastic effects of higher modes. The final base shear force is used to calculate the internal forces and stress of structural components following the force-based design technique. The dynamic analysis method required by NBCC20 assumes the linear behavior of structural materials and relies on the response of vibration modes to evaluate seismic performance. The foundational assumptions underlying this approach can be outlined as follows: (i) the seismic response of a structure during an earthquake can be represented as a linear combination of distinct vibration modes inherent to the structure; (ii) the periodicity of structural vibrations within each vibration mode remains constant throughout the seismic event. Given that the maximum responses across various vibration modes do not coincide during an earthquake, predicting these maximum responses within different structural members is imperative. Accomplishing this necessitates the utilization of statistical methodologies that amalgamate the peak responses derived from different vibration modes. Moreover, these methods must account for potential interaction effects stemming from diverse responses originating from other vibration modes. In this context, the Square Root of the Sum of Squares (SRSS) and the Complete Quadratic Combination (CQC) methods are two viable approaches for estimating the comprehensive structural response. These methods enable aggregating responses from different modes, providing a holistic understanding of structural behavior during a seismic event.

When using the equivalent static method, the base shear value must be reduced to account for the structure's plastic behavior by applying overstrength (R_o) and ductility-related (R_d) factors (see Table 1). Therefore, NBCC20 introduced Equation (1) to determine the equivalent static base shear force (based on the seismic hazard of 2% probability/50 years).

$$V_{base} = S(T_a)M_v\frac{I_E}{R_dR_o}W \quad (1)$$

where T_a is the structures' fundamental period and $S(T_a)$ is the design spectral response acceleration. I_E and M_v represent the importance and higher mode effects factors, respectively. W represents the structures' weight that can be determined by Equation (2).

$$W = DL + 0.25SL \quad (2)$$

where DL is dead load and SL represent snow load.

Table 1. R_d and R_o in different types of SSWs.

Type of SFRS	Force Modification Factor	
Ductile SSW	R_d = 3.5	R_o = 1.6
Moderately ductile SSW	R_d = 2	R_o = 1.4
Conventional SSW	R_d = 1.5	R_o = 1.3

The factored shear force should be raised to consider flexural overstrength, γ_w, since rebars located vertically in the plastic hinge zone may experience high tension stresses due to strain hardening. Therefore, to increase safety against brittle shear failure in ductile SSWs, flexural overstrength is determined by employing a stress of 1.25 f_y in the vertical rebars (f_y is the yield strength of steel rebars) [23]. This is particularly important for components with significant force reduction factors. For ductile SSWs, the flexural overstrength coefficient may be calculated by the ratio of the probable bending moment to the factored bending moment [24]. In multi-degree of freedom SSWs, shear force in the first vibration mode does not increase after flexural yielding occurs in the plastic hinge zone. However, it significantly increases in higher vibration modes as the level of ground motion intensity rises [25]. Hence,

the CSA A23.3-19 requires modifying the factored base shear force to account for the plastic effect of higher modes. Table 2 displays the corresponding coefficients.

Table 2. Coefficient for plastic effects of higher modes.

$T_a \leq T_L$	$T_a \geq T_U$
1.0	$1.0 + 0.25\left(\frac{R_o R_d}{\gamma_w} - 1.0\right) \leq 1.5$ and ≥ 1.0

Where T_L and T_U shall be calculated according to Table 3.

Table 3. Calculation of T_L and T_U.

	T_L	T_U
S(0.2)/S(2.0) < 10.0	0.5 s	1.0 s
S(0.2)/S(2.0) ≥ 10.0	0.2 s	0.5 s

Where S(T) is the design spectral acceleration and is presented for different periods by NBCC20. When a lateral load is applied, the RC component loses its initial stiffness due to cracking and crushing on the tension side of the concrete. CSA A23.3-19 requires employing sectional property reduction factors to address the nonlinear behavior of concrete in the linear analysis of RC members. Table 4 displays the sectional property reduction factors.

Table 4. Proposed sectional effective properties for linear analysis.

Element	Property	Effective Property
Wall	Flexural stiffness Axial stiffness	$EI_e = \alpha_w EI_g$ $EA_{xe} = \alpha_w EA_g$

Where A_g = areas' gross section, E = concretes' modulus of elasticity, A_{xe} = effective axial cross section, I_g = gross section moment of inertia, I_e = effective moment of inertia, and α_w can be regarded as 0.5 for ductile SSWs, as suggested elsewhere [24]. Per capacity-design method regulations, the CSA A23.3-19 offers a framework for establishing a well-designed zone at the base of SSWs to manipulate the formation of plastic hinges. This designated zone must exhibit uniformity concerning the cross-section area, reinforcement detailing, and concrete strength. Notably, designing structures to experience elastic behavior during seismic events can prove uneconomical. By forming the plastic zones within SSWs, a substantial amount of energy dissipation becomes achievable without incurring significant strength deterioration.

The computation of the top displacement of SSWs can be straightforwardly derived by multiplying the total rotation at the base of the shear walls with the wall's height, h_w. Furthermore, research investigations have demonstrated a correlation between the rotational capacity of shear walls and critical factors such as the height of the plastic hinge zone, the ultimate compressive strain of concrete, ε_{cu}, and the ultimate tensile strain of rebars, ε_{smax}, within the plastic hinge zone [26]. Considering this, CSA A23.3-19 mandates that to ensure the ductile performance of SSWs, the inelastic rotational capacity of the shear wall within the plastic hinge zone must surpass the inelastic rotational demand. Inelastic rotational demand in SSWs could be calculated as presented in Equation (3).

$$\theta_{id} = \left(\frac{\Delta_f R_o R_d - \Delta_f \gamma_w}{h_w - \frac{\ell_w}{2}} \right) \geq 0.004 \quad (3)$$

where Δ_f is the factored walls' top displacement. Accordingly, $\Delta_f R_o R_d$ represents the design wall displacement, and $\Delta_f \gamma_w$ is the elastic portion of the wall displacement. The inelastic rotational capacity of the wall is presented in Equation (4).

$$\theta_{ic} = \left(\frac{\varepsilon_{cu} \ell_w}{2c} - 0.002 \right) \leq 0.025 \quad (4)$$

where c is the depth of neutral axis. It should be noted that, within the plastic hinge zone, the flexural rebars' plastic curvature and plastic tension strain change in a linear manner from the maximum level (which is at the point where the first yielding occurs) to zero. However, the plastic tension strain and curvature can be considered uniform at the maximum level to ease the wall deformation calculation [27].

3. An Overview of the Studied Building

The present study evaluated specifically two sets of buildings with 20-story and 15-story configurations located in Vancouver and Montreal, site class C. As seen in Figure 2, these buildings solely rely on SSWs as their SFRS in both primary axes and have four SSWs in the North–South (N-S) direction and two SSWs in the West–East (W-E) direction. Regarding the vulnerability of structures to ground motion acceleration from different angles, the principal objective of this investigation was to evaluate the seismic implications along the North–South axis. The vertical distance between the floors has been set to 3.5 m, leading to a total height of 70 m and 52.5 m for 20-story and 15-story SSWs, respectively. As seen in Figure 2, the buildings have a symmetrical 21 m by 40 m dimension and 200 mm thick RC slabs. The concrete compressive strength, f'_c, and the steel rebar yield strength, f_y, are assumed to be 30 MPa and of 400 MPa, respectively.

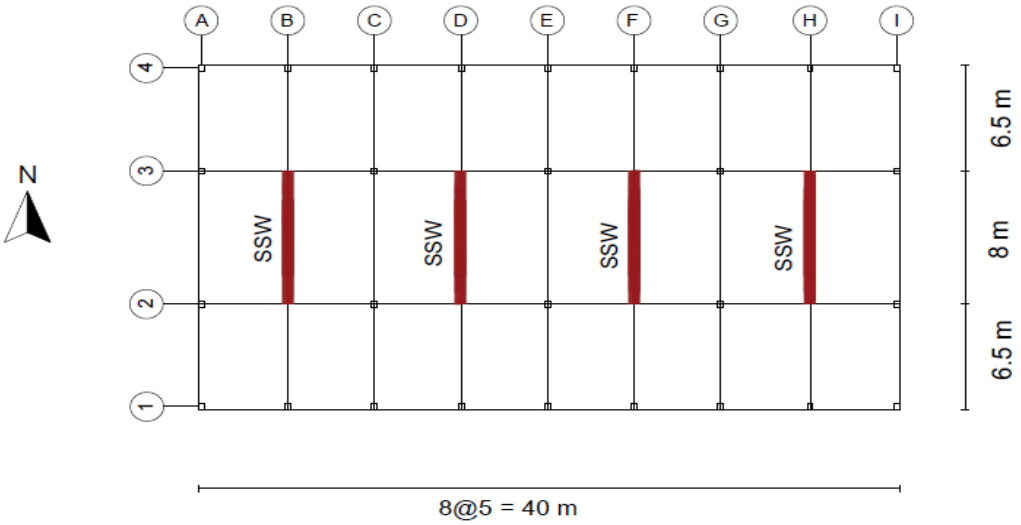

Figure 2. Plan view of the studied building.

The first phase of the study involved designing and detailing SSWs. The base shear was determined through an equivalent static method. This was followed by executing a linear dynamic analysis using SAP2000 software version 19.0.0 [28]. The resulting base shear from the dynamic analysis was then scaled with the base shear obtained from the equivalent static method, as per the provisions of the NBCC20. A similar procedure and design guide can be found elsewhere [3,24]. Figure 2 illustrates the plan view, Figure 3 shows the reinforcement configuration, and Table 5 the reinforcement detailing.

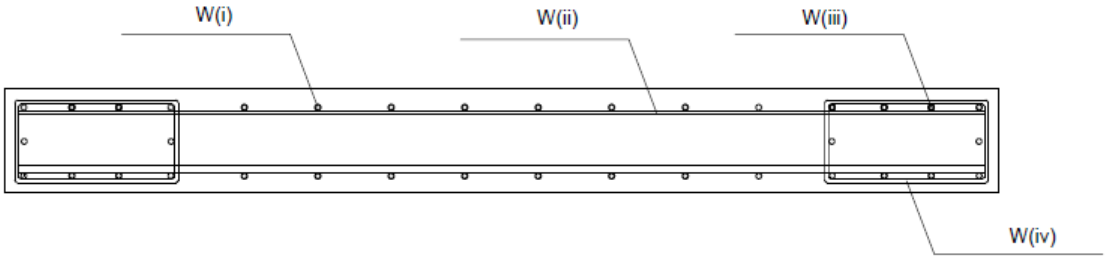

Figure 3. Reinforcement configuration of shear walls.

Table 5. Reinforcement details of shear walls.

		W (i) (mm)	W (ii) (mm)	W (iii) (mm)	W (iv) (mm)	Section Dimension (mm)
West	20-story	15 M @200	15 M @150 15 M @200	2 × 10 30 M in PH region 2 × 10 25 M out of PH region	10 M @150 10 M @200	8000 × 450
	15-story	10 M @200	15 M @200 15 M @250	2 × 8 25 M in PH region 2 × 8 20 M out of PH region	10 M @200 10 M @250	8000 × 400
East	20-story	15 M @200	15 M @200 15 M @250	2 × 8 25 M in PH region 2 × 8 20 M out of PH region	10 M @200 10 M @250	8000 × 450
	15-story	10 M @200	15 M @200 15 M @250	2 × 8 20 M in PH region 2 × 8 15 M out of PH region	10 M @200 10 M @250	8000 × 400

4. Seismic Improvement of SSWs Using EB-FRP Sheets

As discussed in previous sections, ductile shear walls are susceptible to plastic hinge formation at the wall base due to excessive bending and flexural demands experienced during cyclic loads. These loads can lead to reinforcement yielding and concrete crushing at the wall base, which are the primary causes of permanent deformation in these walls. Additionally, higher mode effects can lead to excessive shear force demands for taller shear walls.

On the other hand, ACI 440.2 R-17 [29] introduces specific strengthening configurations using EB-FRP composites to address these weaknesses in SSWs. The guideline specifies using vertical EB-FRP composites for flexural strengthening, horizontal EB-FRP for shear strengthening, and wrapping FRP for confinement improvement and avoiding debonding failure. Accordingly, this study has adopted its proposed strengthening configurations based on a combination of the schemes suggested by ACI 440.2 R-17 to find an effective configuration for reducing residual deformation in SSWs.

Incorporating vertical EB-FRP sheets to enhance the flexural resistance of SSWs poses a primary concern with regard to FRP debonding, owing to the concrete's vulnerability in tension [30]. Several studies have recommended resorting to diverse anchorage systems to forestall the premature debonding of EB-FRP [31,32]. Despite this, the execution of experimental examinations to authenticate the effectiveness of these systems during seismic events limits their application. As a reliable solution, ACI 440.2 R-17 has put forward the utilization of fully wrapped FRP in regions prone to debonding, particularly in plastic hinge zones [3,29]. In analytical procedures, according to Equation (5), ACI requires designers to restrict the effective strain of FRP sheets, ε_{fd}, to avoid debonding failure.

$$\varepsilon_{fd} = 0.41\sqrt{\frac{f'_c}{nE_f t_f}} \leq 0.9\varepsilon_{fu} \quad (5)$$

In Equation (5), f'_c and n denote the concrete compressive strength and the number of FRP layers, respectively; E_f and t_f are the modulus of elasticity and the thickness of FRP sheets, respectively; ε_{fu} represents the rupture strain of FRP composites.

This study considers three unique schemes aimed at fortifying vulnerable flexural and compressive cracking regions within medium- to high-rise SSWs. The primary goal is to enhance the seismic resilience of these crucial SFRS. The present study comprehensively assesses and interprets the effectiveness of these schemes in reducing residual deformation in SSWs. Also, it is crucial to prevent brittle shear failure prior to the yielding of bending moment reinforcement.

Consequently, as a means of enhancing the load-carrying capacity, ductility, and shear strength of SSWs, fully wrapped FRP has been implemented. This implementation is primarily aimed at improving the resistance against debonding failure in accordance with the recommendations of the ACI. Moreover, the issue of concrete crushing due to high compressive strain in the plastic hinge zone is a formidable challenge in slender SSWs during cyclic events. However, this challenge can be addressed through additional confinement and the complete wrapping of the shear wall base. In the first retrofitting scheme, hereinafter R1-SSW, vertical FRP layers were added to both surfaces of the SSW to enhance the bending capacity of the shear wall in addition to the FRP wrapping. In the second configuration, R2-SSW, from both vertical edges, the first 15% of SSW's length on both faces was fully covered by two layers of vertical EB-FRP, followed by one layer of vertical EB-FRP in the adjacent 15% from the base to the top of the walls. In the third proposed scheme, R3-SSW, three layers of vertical EB-FRP were attached to the first 15% of the length of SSW from vertical edges on both sides. An additional layer of FRP wrapping was also used in its plastic hinge zone. A similar retrofitting configuration in coupled shear walls has been previously used elsewhere [3]. In this research study, with the unreinforced wall being referred to as the control wall and labeled as C-SSW, a total of 16 distinct SSWs were evaluated. Also, FRP sheets with a tensile strength of 1355 MPa, a tensile modulus of 115,700 MPa, and a thickness of 1.3 mm were used. The impact of concrete cracking on the bonding behavior of EB-FRP composites is not considered. Figure 4 shows the different configurations considered in this study.

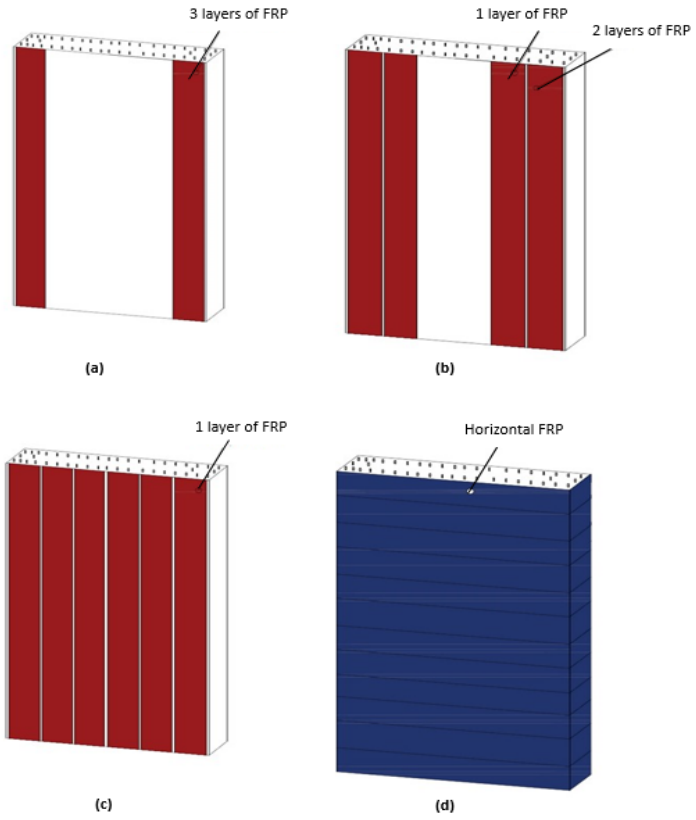

Figure 4. Different strengthening schemes used in this study: (**a**) R3-SSW; (**b**) R2-SSW; (**c**) R1-SSW; (**d**) FRP wrapping of shear walls.

5. Nonlinear Time History Analysis of SSWs

The NLTH analysis technique is widely acknowledged as one of the most accurate and practical approaches for evaluating the behavior of structures under cyclic seismic forces. Therefore, NLTH analysis using RUAUMOKO 2D software [33] has been carried out in this study following the provisions of structural commentaries [34].

5.1. Model Assumptions

The slender walls considered in this study can withstand the forces induced by ground motions through flexural action, akin to the resilience displayed by cantilevered RC beams. In particular, the analysis of shear deformation should consider a linear elastic approach as specified by capacity-design regulations that pertain to ductile shear walls [35]. RUAUMOKO 2D software, a finite element-based computational tool, boasts an expansive array of beam and beam–column components expressly designed to simulate flexural frame-like components. The plastic behavior of these components is based on the Giberson one-component model [36]. In this model, the inelastic tendencies occur only at both ends, while the central elastic portion remains unaffected. Beam–column members have a significant advantage as they can handle both axial loads and bending moments, which is a critical factor in assessing the performance of shear walls during seismic events. Therefore, quadratic beam–column members were used in the centroid of both strengthened and control shear walls to model them in this study. Figure 5 displays the modeling of SSWs assessed in this investigation.

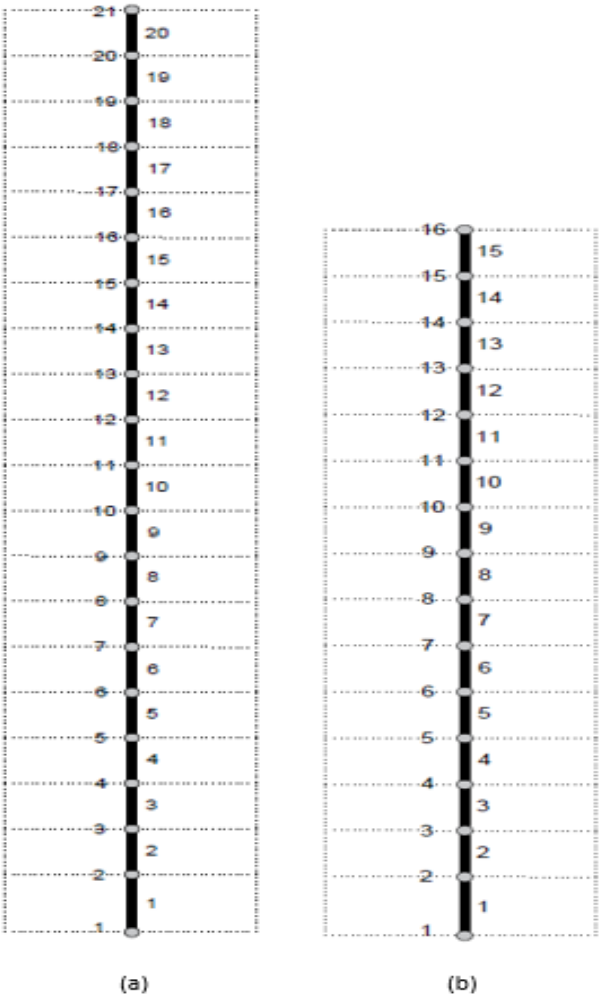

Figure 5. Member and node modeling of (**a**) 20-story shear wall; (**b**) 15-story shear wall.

In addition to the advantages mentioned above, plastic hinges on both ends of this member allow the wall to experience plastic response throughout its height during the NLTH analysis. This insight is even more critical when considering the impact of higher modes on tall shear walls, which can create a second set of plastic hinges in the upper levels [37]. However, it is important to acknowledge that the selection of member height can affect the model. This is because inelastic behavior is confined to the ends of the components, neglecting potential distributed plasticity. Quadratic beam–column members have previously been used to model shear walls [3,38]. In order to address the impacts of axial forces and bending moments in SSWs, Xtract software v2.6.0 [39] was employed to create the interaction graph. The linear elastic response of the FRP materials bonded to the RC members was determined by their manufacturing attributes. To model reinforcing rebars' nonlinear response, a bilinear model with strain hardening was considered. For confined and unconfined concrete, the model presented by Mander et al. [40] was applied, while the Lam and Teng [41] model was utilized to view curvature enhancement in concrete with FRP confinement. While this study focuses primarily on the nonlinear sectional properties of reinforced concrete (RC) members, it is acknowledged that the seismic performance of concrete structures is heavily influenced by the material properties used in construction. Key factors, including the type and quality of aggregates, cement grade, and specific mix design, are fundamental in shaping the structures' ductility, strength, and energy dissipation capacities. Notably, the response of aggregates under dynamic loads is critical for understanding the integrity and cracking behavior during seismic events. Further details on these aspects are extensively discussed in the existing literature [42]. Also, the lumped mass model was employed due to the assumption that all floors are rigid and thick to produce diaphragm effects. This model assumes that the whole mass of the building is consolidated at the nodes. The mass matrix will only be affected by nodal weights, M_i, on the diagonal elements and, typically, the elements related to rotational degrees of freedom are considered to be zero. So, each diagonal element only corresponds to one translational degree of freedom of the lumped mass. Equation (6) represents the lumped mass matrix, M, in an n-story SSW.

$$\mathrm{M} = \begin{bmatrix} M_1 & & & & \\ & M_2 & & & \\ & & \ddots & & \\ & & & M_{n-1} & \\ & & & & M_n \end{bmatrix} \tag{6}$$

The ductility-based model, using the data suggested by McNeice [43], simulated the decay in RC concrete strength caused by ground motion loading. Furthermore, the large displacement technique was used in order to account for geometric nonlinearity. This method involves updating the nodal coordinates and component stiffnesses during each time step to accommodate axial forces and geometry changes. This enables the analysis of structures experiencing significant displacements [44].

This study used the Q-HYST hysteresis model [45] for the nonlinear response of strengthened and control SSWs to the ground motions. An experimental constant, α, controls the unloading stage of Q-HYST, which is adopted from the experimental studies available in the literature [43]. The stiffness degradation in this model is controlled by Equation (7).

$$K_u = K_o \left(\frac{d_y}{d_m} \right)^{\alpha} \tag{7}$$

where K_u is the degraded stiffness through the unloading stage, K_o is the initial stiffness in the loading stage, and d_y and d_m are yielding and ultimate displacement. This hysteresis model has been used in other investigations and has shown its capability to replicate the plastic response of RC components under seismic loading [38].

5.2. Damping Assumptions

NLTH is a step-by-step systematic approach for solving the fundamental equation of motion (Equation (8)) of a given structure.

$$\mathrm{M}\left(\ddot{X}_{(t)}+\ddot{u}_{(t)}\right)+\mathrm{C}\dot{X}_{(t)}+\mathrm{K}X_{(t)}=0 \tag{8}$$

where $\ddot{X}_{(t)}$, $\dot{X}_{(t)}$, and $X_{(t)}$ denote the acceleration, velocity, and displacement of the structure, respectively; M represents the mass matrix; C and K denote the damping and stiffness matrices; and $\ddot{u}_{(t)}$ represents the ground acceleration.

Choosing an appropriate damping model is crucial to correctly evaluate a structure's nonlinear behavior. The Rayleigh model expressed in Equation (9) is a highly adopted technique in the literature due to its ability and is used in this study.

$$\mathrm{C}=\alpha\mathrm{M}+\beta\mathrm{K} \tag{9}$$

In Equation (9), α and β are constant damping factors proportional to the mass and stiffness matrices. For a structure with several degrees of freedom in each vibration mode with vibration frequency, ω_{i}, the damping ratio, ξ_{i}, can be calculated using Equation (10).

$$\xi_{\mathrm{i}}=\frac{1}{2}\left(\frac{\alpha}{\omega_{\mathrm{i}}}+\beta\omega_{\mathrm{i}}\right) \tag{10}$$

As per Equation (10), at low frequencies, damping proportional to mass is dominant, while, at high frequencies, damping proportional to stiffness is dominant.

In the Rayleigh damping model, selecting two vibration modes along with their corresponding damping ratios is standard practice. In typical applications involving time-domain operations, Rayleigh damping is commonly employed to impart damping characteristics that exhibit a notably diminished sensitivity to frequency variations. Despite the inherent frequency-dependent nature attributed to Rayleigh damping, its parameters can be judiciously chosen within a specific range, aiming to mitigate the extent of frequency-related influences to the greatest extent achievable. On the other hand, selecting very low frequencies (proportional to the mass matrix) results in excessive damping force, which is unsuitable for NLTH analysis. These modes should be chosen strategically to provide an appropriate and balanced representation of the system's damping behavior across the frequency spectrum (different vibration modes) [46]. This ensures that the damping ratios are not skewed towards particular frequency ranges, preventing the issues mentioned earlier with excessive damping at low frequencies. Accordingly, this research study employed the Rayleigh damping technique, which incorporated a critical damping rate of 5% for modes 1 and 10. This methodology has been previously detailed and used elsewhere [3,47].

5.3. Selection and Scaling of the Ground Motions

All selected ground motions for NLTH analysis must conform to the designated characteristics that correspond to their site-specific seismic hazard level. These characteristics include the fault distance to the building site, magnitude, and fault plate tectonic state. In Canada, design seismic hazard levels are periodically updated by NBCC as a function of peak ground acceleration, PGA, peak ground velocity, PGV, and spectral accelerations, Sa, for six distinguishing vibration periods. Currently, NBCC20 is tracking the sixth generation of the seismic hazard model [48], based on a 2% probability of exceedance in 50 years. This version exhibits a considerable increase in the hazard level of site category C (pertaining to building sites in this research) compared to the last version, as depicted in Figure 6.

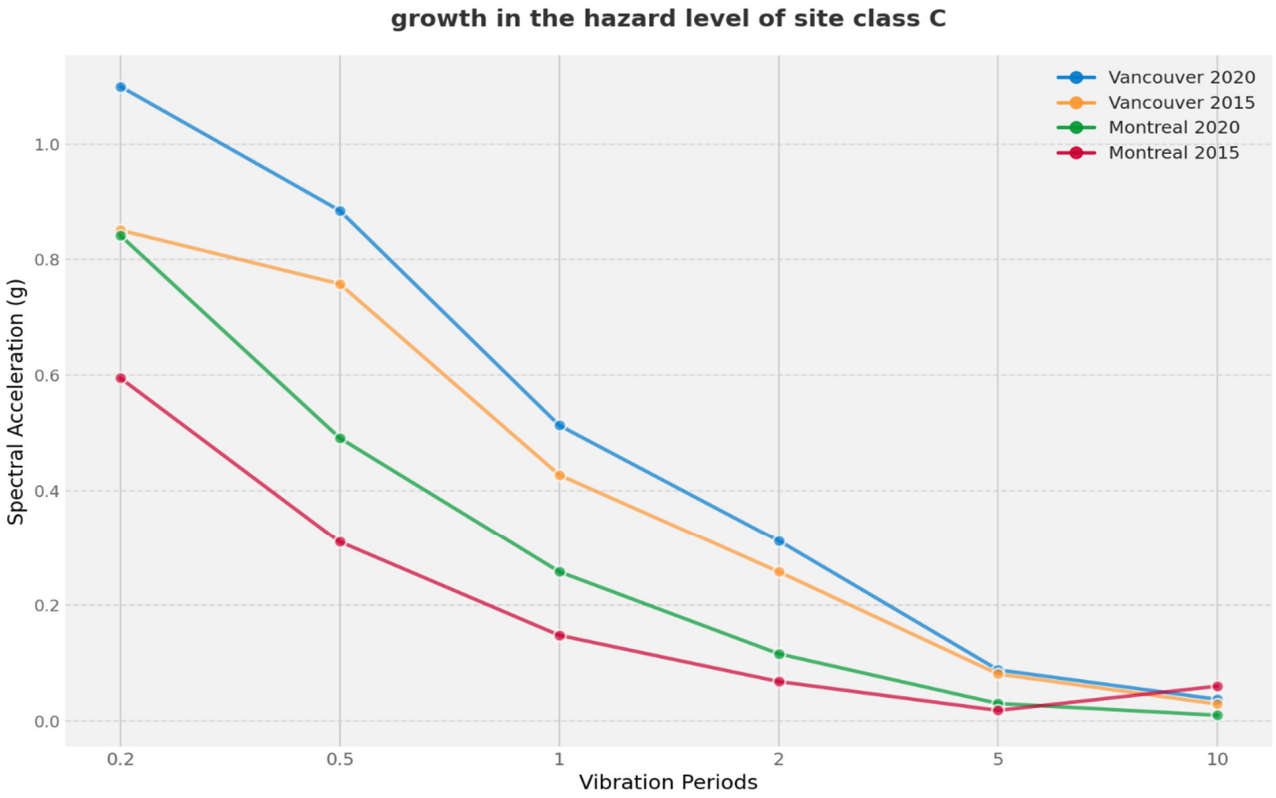

Figure 6. Growth in the hazard level of site category C.

Ground motions have profound differences in the cities in the western Canadian and eastern Canadian seismic zones. As a matter of fact, ground motions in Montreal have a higher frequency content than ground motions in Vancouver [49]. In contrast, Vancouver has typical earthquakes with longer durations specially due to the Cascadian earthquake's occurrence (M > 8) on Canada's west coast [50]. Accordingly, in order to accurately ascertain the magnitude–distance (M-R) scenarios of ground motions that align with the hazard level of a given city, it is imperative to perform a de-aggregation of the seismic hazard analysis pertaining to the aimed city. The findings of the de-aggregation analysis indicate that, in the case of Vancouver, three distinct hazard M-R scenarios must be taken into consideration. Similarly, for Montreal, two scenarios need to be accounted for [48,51].

Because of the deficiency of ground motions conforming with the seismic hazard level of eastern Canada, artificial earthquakes developed by Atkinson [50] are utilized in this research study. The process of choosing and scaling time histories was carried out in line with NBCC guidelines, utilizing the technique recommended by Tremblay et al. [52]. Per the guidelines outlined by the structural commentaries [34], it is required that a minimum of five ground motions be selected for each scenario, with a total of no less than eleven ground motions per city. As such, eleven ground motions have been chosen from the aforementioned source for the city of Montreal, while fifteen ground motions have been selected for Vancouver as detailed in Tables 6 and 7, respectively. The response spectra for the scaled time histories are presented in Figure 7, depicting Montreal and Vancouver.

Figure 8 illustrates variations in earthquake record content for different ground motion scenarios.

Table 6. Description of selected earthquakes in Montreal.

Scenario	Rec. No.	PGA (g)	Duration (s)	Period Range (s)	Event Type
M = 6 10 < R < 30	East 1	0.322	43.59	0.2–1	Crustal
	East 2	0.645	43.59		
	East 3	0.423	43.59		
	East 4	0.451	47.53		
	East 5	0.301	47.53		
M = 7 15 < R < 100	East 6	0.478	51.12	0.5–2.42	Crustal
	East 7	0.410	51.12		
	East 8	0.308	51.12		
	East 9	0.331	57.35		
	East 10	0.248	57.35		
	East 11	0.299	57.35		

Table 7. Description of selected earthquakes in Vancouver.

Scenario	Rec. No.	PGA (g)	Duration (s)	Period Range (s)	Event Type
M = 6.5 10 < R < 30	West 1	0.475	49.30	0.2–0.8	Crustal
	West 2	0.483	49.30		
	West 3	0.503	49.30		
	West 4	0.497	53.63		
	West 5	0.559	53.63		
M = 7.5 15 < R < 100	West 6	0.391	102.02	0.3–1.5	In-slab
	West 7	0.430	102.02		
	West 8	0.351	102.02		
	West 9	0.289	93.39		
	West 10	0.423	93.39		
M = 9 100 < R < 200	West 11	0.137	309.42	1–4	Cascadia subduction
	West 12	0.132	309.42		
	West 13	0.173	309.42		
	West 14	0.146	309.42		
	West 15	0.167	309.42		

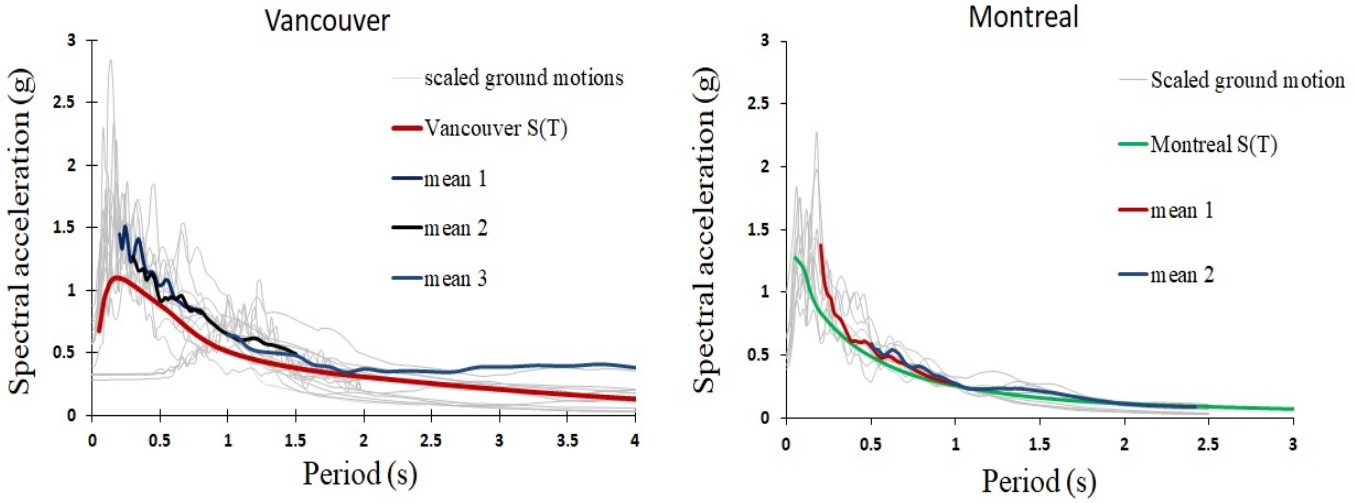

Figure 7. Response spectra for scaled ground motions.

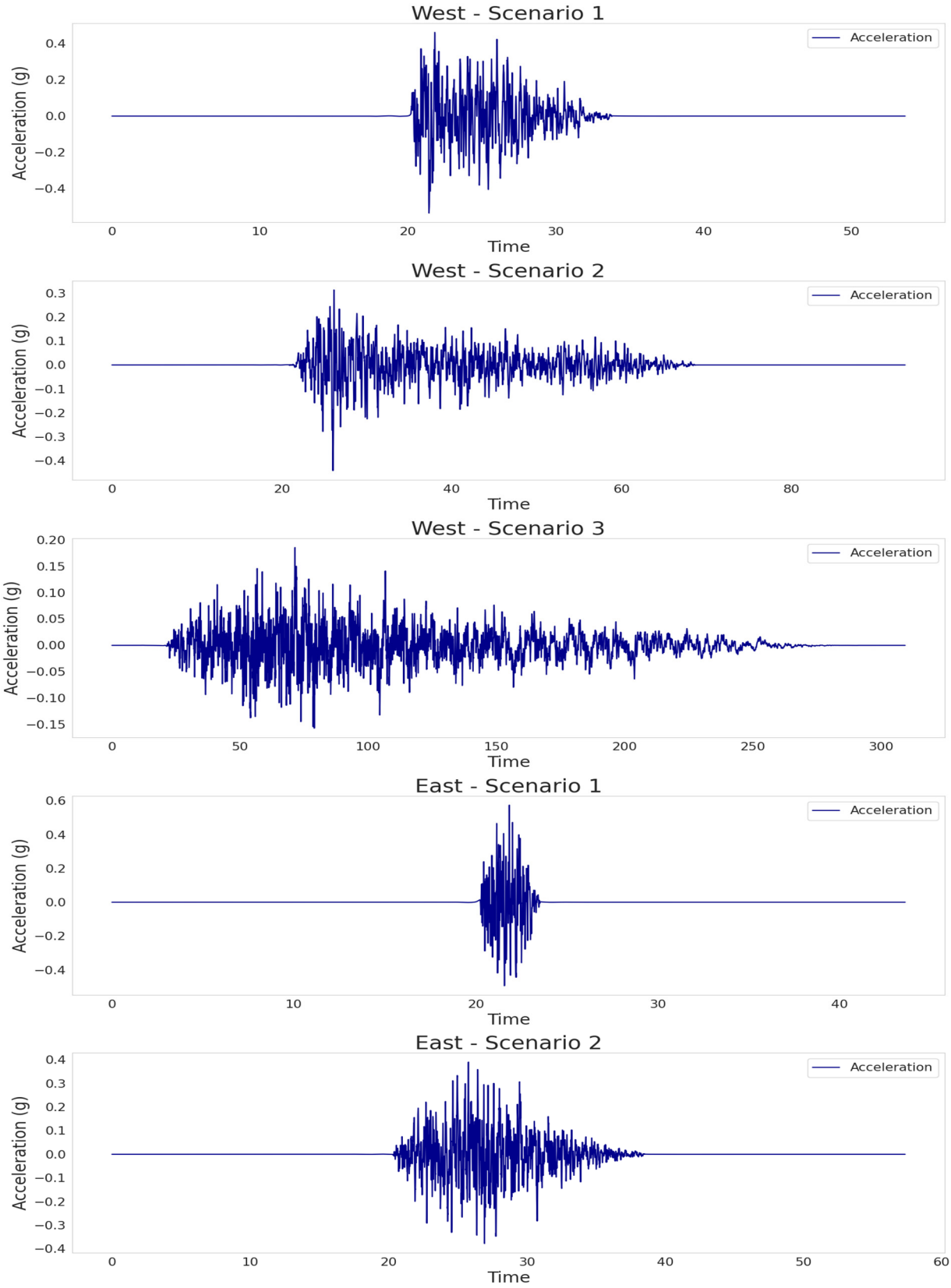

Figure 8. Variation in earthquake record content for different ground motion scenarios.

6. Interpretation of the Results

The present study aimed to evaluate the efficiency of using EB-FRP sheets in enhancing the seismic resilience of SSWs by decreasing the residual displacement. This was achieved

by means of nonlinear time history analysis of different strengthening schemes of 20- and 15-story SSWs located in the Western and Eastern Canadian seismic zones. This study also discusses the influence of applied strengthening schemes on inter-story drift ratio (IDR), shear force demand, and bending moment demand in shear walls. Nevertheless, assessing residual displacement in reinforced concrete structures is a contentious issue intricately linked to the specific aim under examination [3]. In this regard, ASCE-7-22 [53] used IDR as a metric to evaluate structures' self-centering capability and restricted residual inter-story drift ratio (RIDR) in structures taller than 73 m to 1%. Hence, this study capitalized on the RIDR as a metric to assess the effectiveness of the proposed reinforcement strategies in reducing residual displacement in SSWs.

6.1. Inter-Story Drift Ratio (IDR)

The NBCC20 regulations restrict IDR demand to 2.5%. However, in seismic zones with low-frequency ground motions, the IDR profiles of RC shear walls can diverge from the one derived through linear analysis due to concentrated plastic rotation at the base. Thus, a thorough assessment of IDR is crucial to anticipate unexpected demands.

6.1.1. Walls in Vancouver

The NLTH analysis results for a 20-story SSW in Vancouver reveal a significant influence of ground motion frequency content (across various scenarios) on the IDR. Figure 9 displays the mean peak IDR values for different scenarios and strengthening schemes. Notably, the dominant events driving the flexural response of SSWs in this region are Cascadia subduction events (M9). These events are characterized by their low-frequency content and extended durations, capable of exciting the wall's first vibration mode. While the peak mean IDR for this scenario did not exceed the 2.5% limit, it still stood at approximately twice the peak mean IDR envelope value of all ground motions. Additionally, the influence of higher modes becomes evident in the M6.5 scenario, where ground motions exhibit higher frequencies and there is a possibility for a second plastic hinge in the upper levels. Meanwhile, the results show that using EB-FRP sheets could decrease the peak IDR in this wall up to 8, 11, and 17% in R1-SSW, R2-SSW, and R3-SSW, respectively.

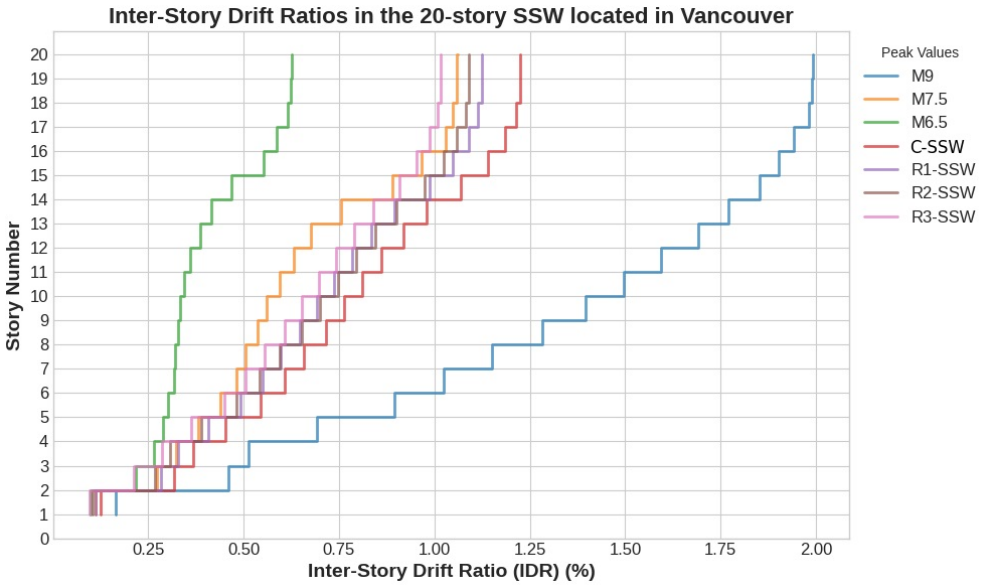

Figure 9. Mean peak IDR values for different scenarios and strengthening schemes in 20-story SSW located in Vancouver.

The efficiency of strengthening configurations demonstrated a more significant impact in the 15-story SSW, where the maximum reduction in R3-SSW reached 28%. This comparison with the R3-SSW in the 20-story wall indicates that the effectiveness of im-

plementing EB-FRP sheets in shear walls diminishes as the height of the walls increases. Also, shorter SSWs displayed a comparatively lower sensitivity to the effects of higher modes. Similar findings have been reported elsewhere [3]. Additionally, the suggested strengthening schemes resulted in a reduction in IDR by up to 18% in R2-SSW and 13% in R1-SSW. Figure 10 illustrates the mean peak IDR in the 15-story SSW located in Vancouver for different scenarios.

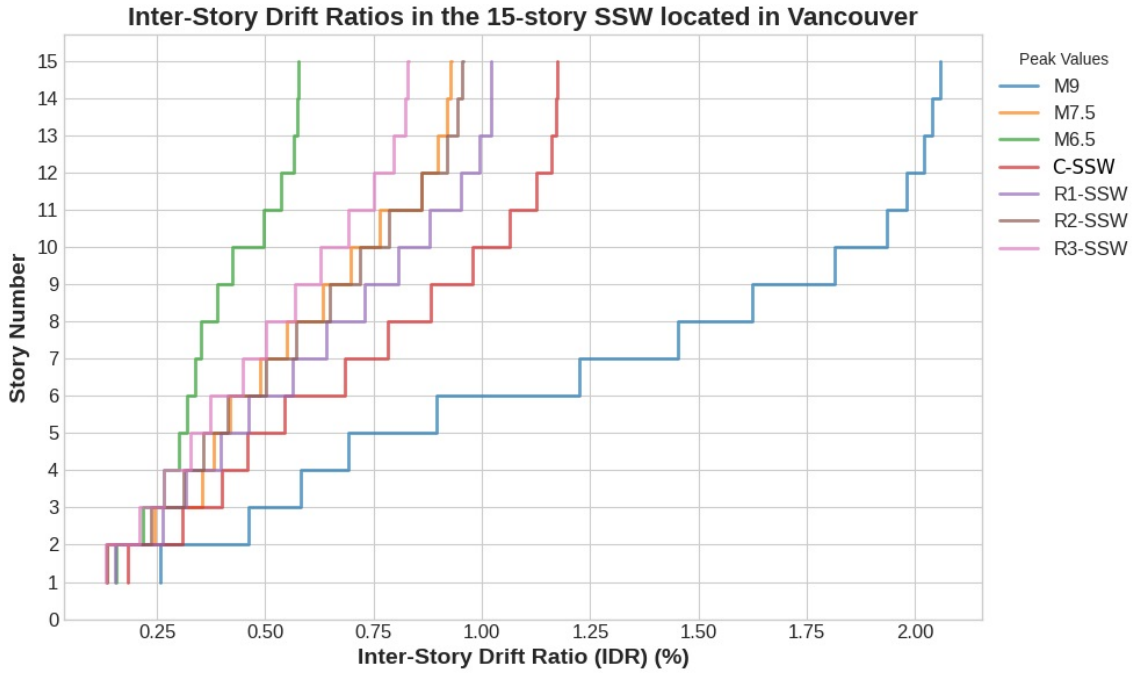

Figure 10. Mean peak IDR values for different scenarios and strengthening schemes in 15-story SSW located in Vancouver.

6.1.2. Walls in Montreal

While Western Canada does experience low-frequency seismic events with longer durations, Montreal, on the other hand, does not encounter such low-frequency seismic events. Notably, the results of the NLTH analysis revealed a reduced IDR in a 20-story SSW in Montreal compared to a corresponding wall in Vancouver due to the lower seismic activity level. As illustrated in Figure 11, both the M6 and M7 scenarios observed in Montreal highlight the impact of higher modes on the wall structure, which could potentially result in the development of a secondary plastic hinge at upper levels. This phenomenon is observed within the wall's 60% to 70% height range. However, due to this region's relatively low seismic activity, the flexural demands on these walls are lower than their capacity. Nonetheless, the likelihood of secondary plastic hinge formation at upper levels increases in taller walls where the higher frequency effect becomes more pronounced. The NLTH analysis results of IDR revealed that both M7 and M6 scenarios in 20-story SSWs reflect the effects of higher modes, but the M7 was the prevailing scenario in Montreal, where the wall experienced an average peak IDR of approximately 0.25%, while the mean peak IDR for all ground motions stood at around 0.23%. Furthermore, the implementation of strengthening schemes demonstrated the potential to reduce IDR in this wall by margins up to 5%, 8%, and 13% in R1-SSW, R2-SSW, and R3-SSW, respectively. Furthermore, the use of the proposed strengthening configurations can decrease the fluctuations in the mean IDR envelope within this wall.

The NLTH analysis results indicate that higher modes' influence on the 15-story wall is relatively limited compared to the taller shear wall. Although forming a second plastic hinge between levels 9 and 12 appears possible in M6 events, the ground motion intensity in this scenario falls significantly below the wall's flexural capacity. Conversely,

the M7 scenario emerges as the dominant event for this wall, exhibiting a maximum IDR of approximately 0.53% (see Figure 12). However, this value is considerably lower than the NBCC20 limit for ductile shear walls. Furthermore, the findings suggest that the recommended strengthening strategies are more effective in reducing the IDR of a 15-story wall than a 20-story one. Notably, the S3-CSW configuration achieved the most significant IDR reduction, reaching 21%, while mean IDR decreases of 12% and 9% were observed for the S2-CSW and S1-CSW configurations, respectively.

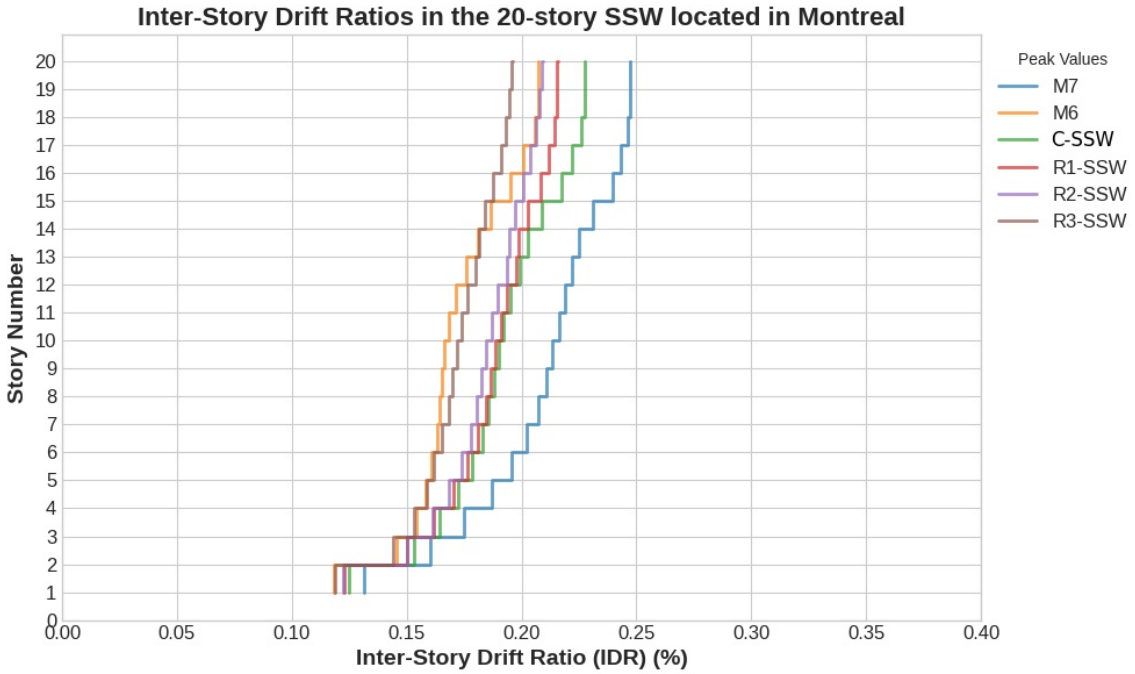

Figure 11. Mean peak IDR values for different scenarios and strengthening schemes in 20-story SSW located in Montreal.

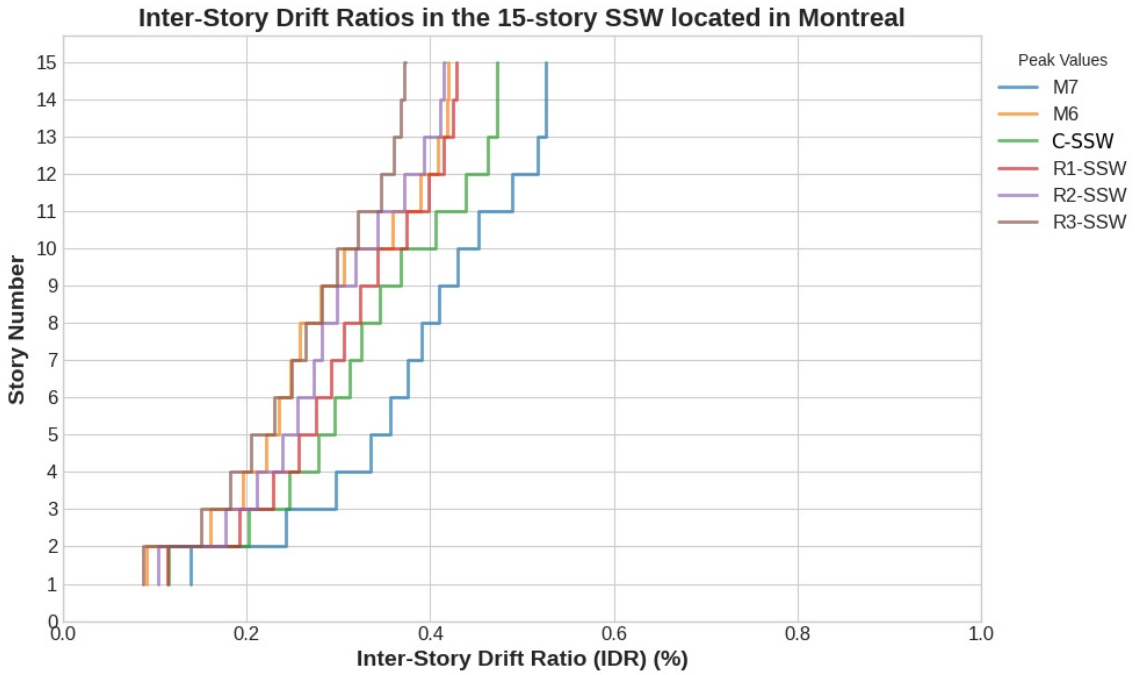

Figure 12. Mean peak IDR values for different scenarios and strengthening schemes in 15-story SSW located in Montreal.

6.2. Residual Displacement of Walls

6.2.1. Walls in Vancouver

The presence of severe ground motions characterized by low frequencies and prolonged durations in Western Canada resulted in significant residual displacements in SSWs within this region. As shown in Figure 13, the findings revealed that the maximum RIDR in a 20-story SSW occurred during earthquake 14, wherein the wall experienced a notable 1.36% RIDR. Figure 14 also shows the RIDR values of 15-story shear wall for all ground motions in Vancouver. This heightened residual value can be attributed to the extended duration of Cascadia events, leading to structural fatigue due to a substantial number of loading and unloading cycles. Furthermore, in addition to the Cascadia events (M9), in-slab events (M7.5) exhibited a noteworthy level of RIDR. This can be attributed to the significant energy generated by these events in lower vibration modes, resulting in substantial flexural forces at the base of the shear walls, consequently leading to notable residual displacements.

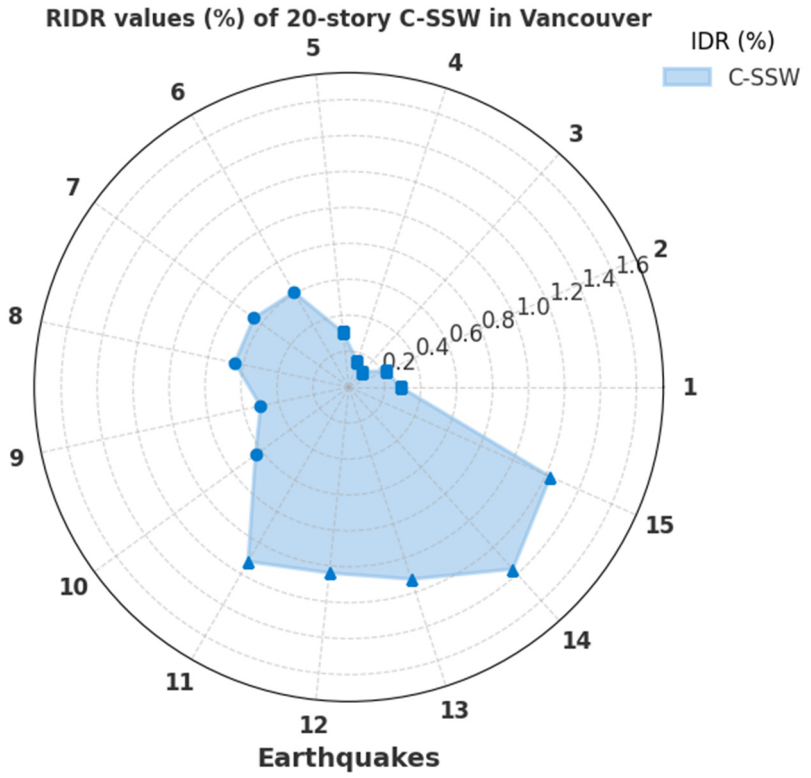

Figure 13. Maximum RIDR in 20-story C-SSW for different scenarios located in Vancouver.

The proposed strengthening strategies yielded significant reductions in RIDR for both 20-story and 15-story shear walls, with the 15-story wall experiencing a more pronounced effect. According to the results, R3-SSW achieved a remarkable 39% reduction in RIDR for the 15-story wall, compared to a 22% reduction in the 20-story wall. This disparity can be attributed to the greater efficiency of EB-FRP in enhancing stiffness in shorter walls, a trend that previous studies have corroborated [3,54].

Furthermore, R2-SSW demonstrated substantial reductions of up to 29% in the 15-story wall and 14% in the 20-story wall. In contrast, R1-SSW had a comparatively milder impact on reducing RIDR, resulting in reductions of 15% for the 15-story shear wall and 8% for the 20-story shear wall. Figures 15 and 16 illustrate a reduction in RIDR due to the strengthening schemes, for all ground motions in 20-story and 15-story SSWs, respectively.

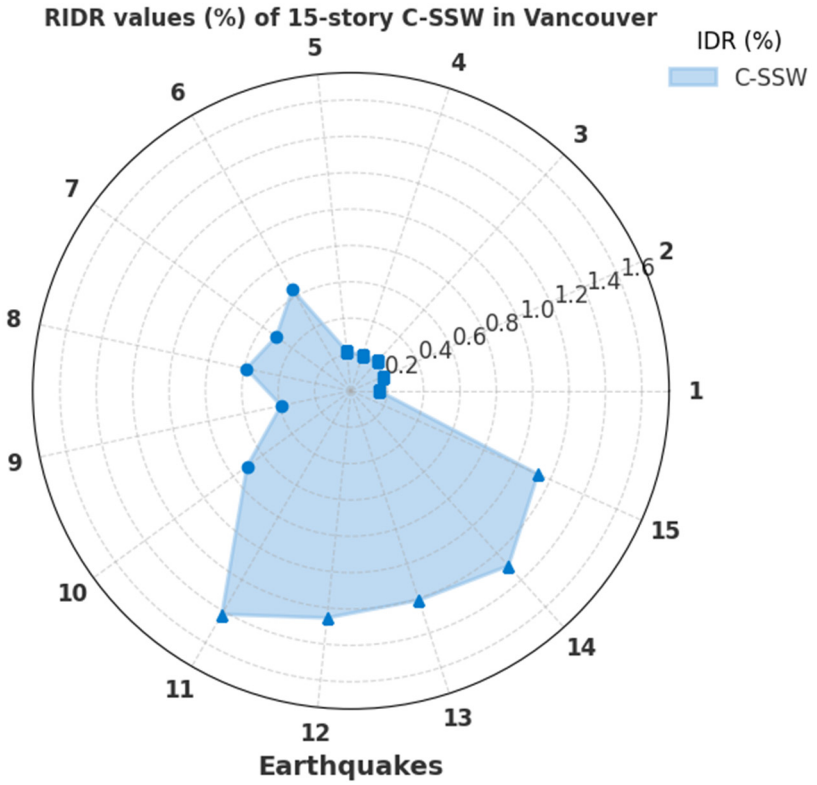

Figure 14. Maximum RIDR in 15-story C-SSW for different scenarios located in Vancouver.

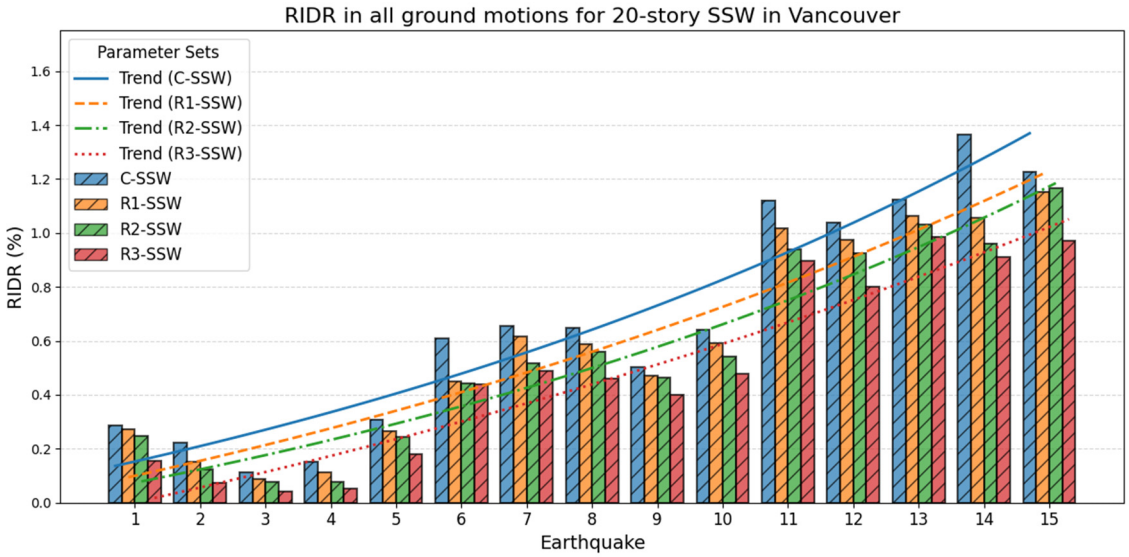

Figure 15. Reduction of RIDR in 20-story SSW located in Vancouver, due to strengthening schemes, in all scenarios.

6.2.2. Walls in Montreal

The findings reveal a notable reduction in wall damage within Eastern Canada, attributed to their reduced susceptibility to destruction owing to their exposure to high-frequency, low-magnitude earthquakes incapable of inducing substantial flexural strains in structures (see Figures 17 and 18). The prevalence of higher-frequency seismic waves in these areas allocates a more significant proportion of seismic energy to the higher vibration mode range, thereby diminishing the likelihood of plastic hinge formation at the base of the walls.

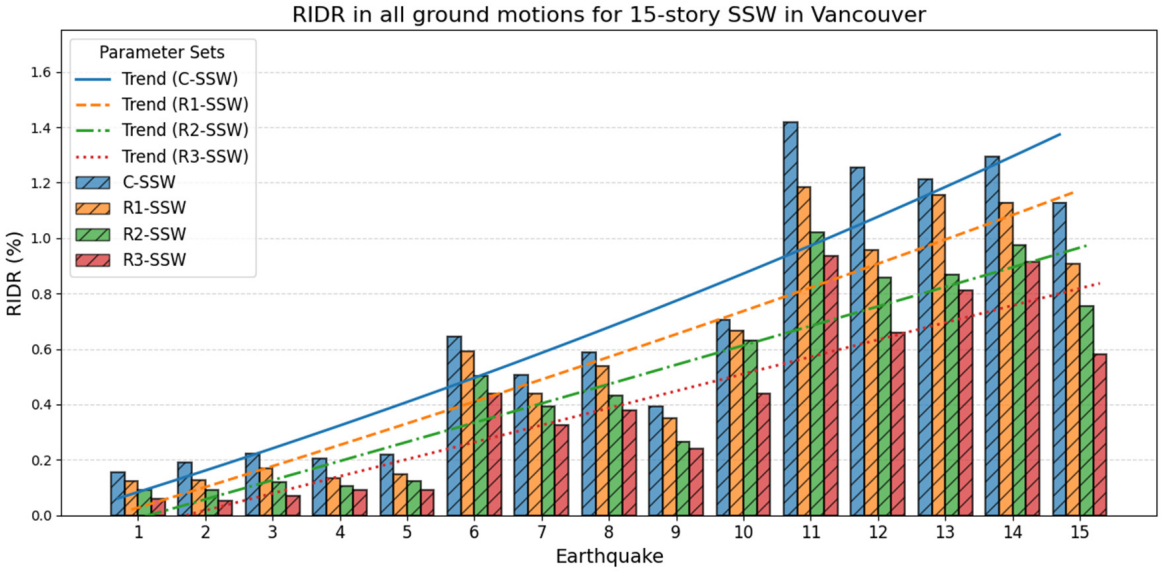

Figure 16. Reduction of RIDR in 15-story SSW located in Vancouver, due to strengthening schemes, in all scenarios.

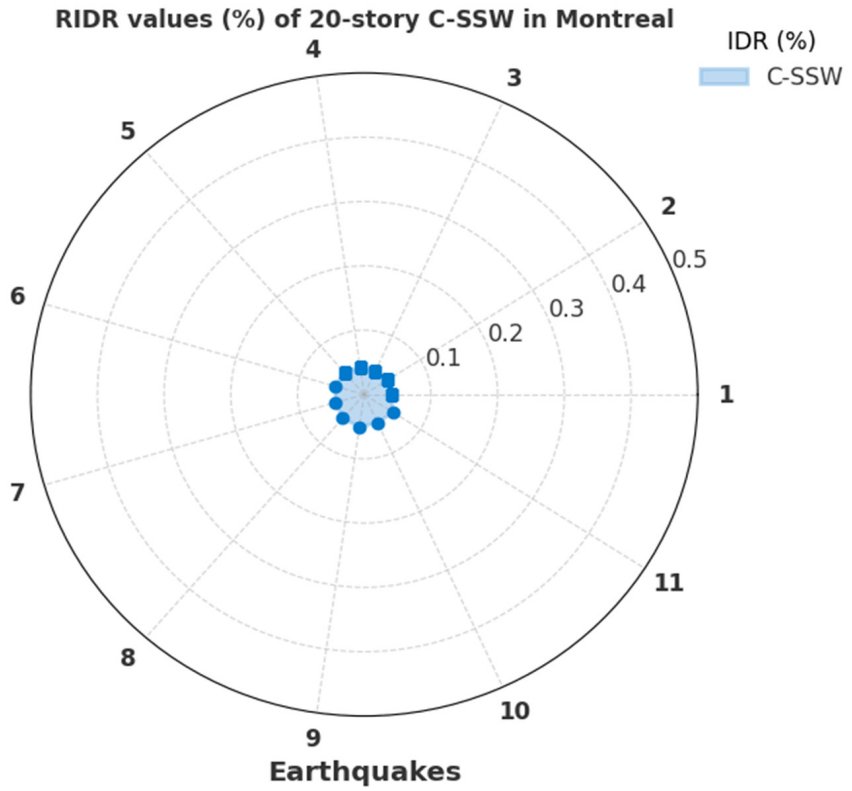

Figure 17. Maximum RIDR in 20-story C-SSW for different scenarios located in Montreal.

As shown in Figure 19, the residual displacements of a 20-story SSW in Montreal remain remarkably low when subjected to seismic-dominant scenarios. In contrast, the 15-story SSW exhibits slightly higher residual displacements compared to its taller counterpart (refer to Figure 20). Nevertheless, these values remain significantly lower than those observed in the corresponding wall located in Vancouver. In the case of the 15-story SSWs in Montreal, denoted as R1-SSW, R2-SSW, and R3-SSW, the application of EB-FRP sheets resulted in RIDR reductions of 31%, 49%, and 66%, respectively. However, it is worth noting that the seismic behavior of the 20-story SSW appears to be predominantly elastic,

making the use of EB-FRP sheets in this wall less justifiable. Previous studies have also demonstrated that high-rise slender shear walls in Eastern Canadian seismic zones tend to exhibit predominantly elastic responses to ground motions.

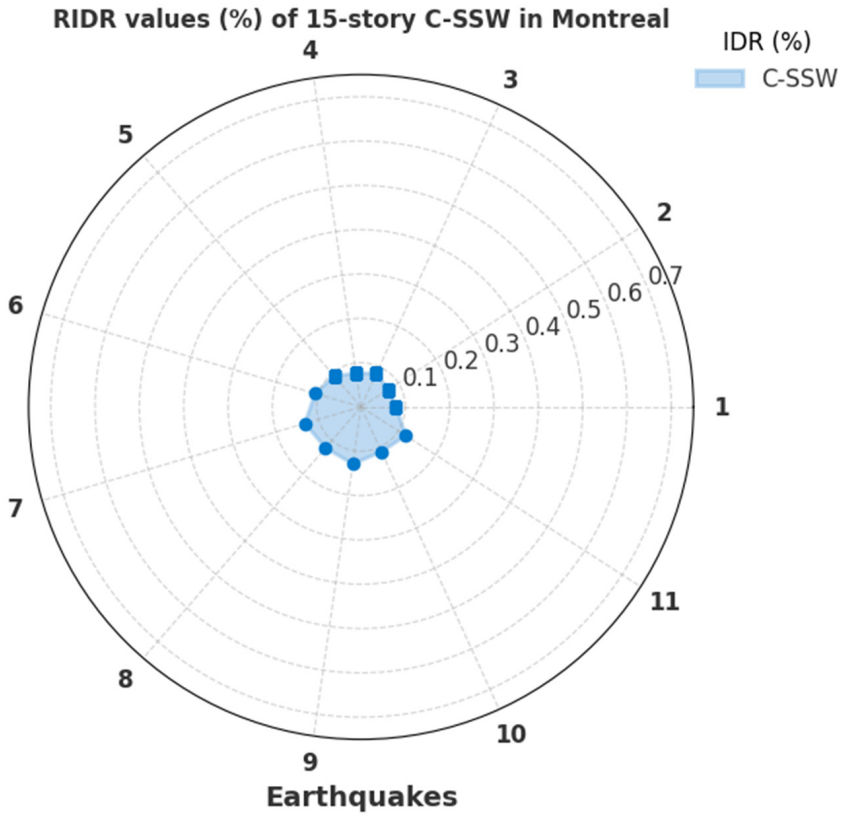

Figure 18. Maximum RIDR in 15-story C-SSW for different scenarios located in Montreal.

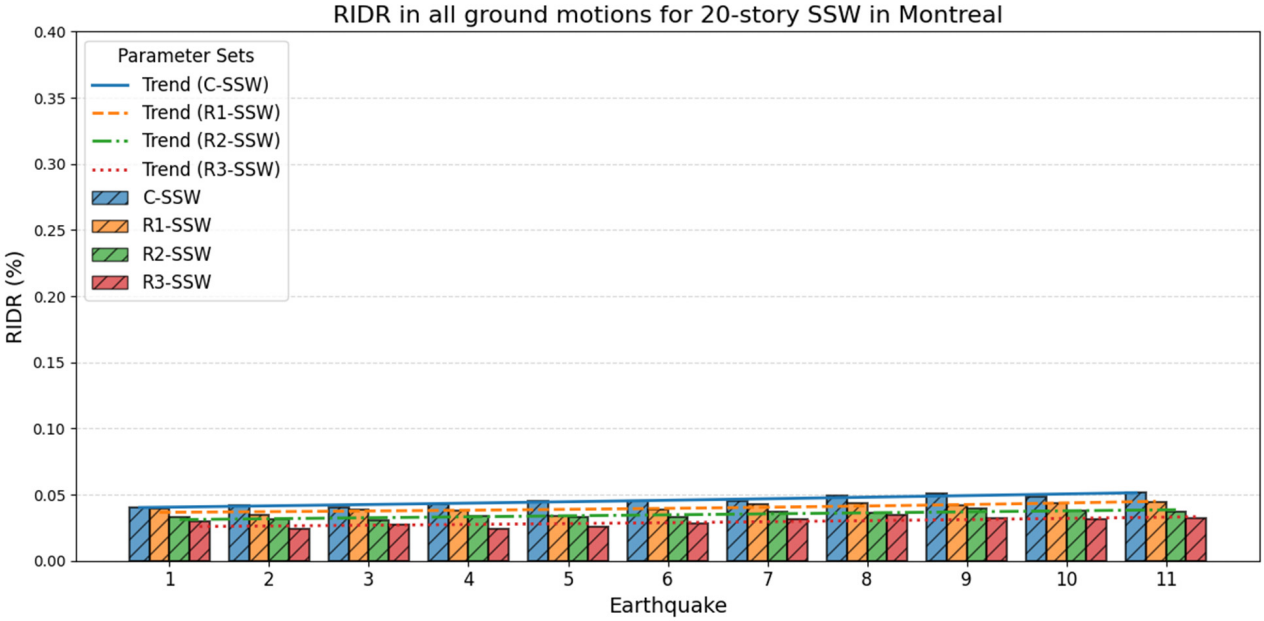

Figure 19. Reduction of RIDR in 20-story SSW located in Montreal, due to strengthening schemes, in all scenarios.

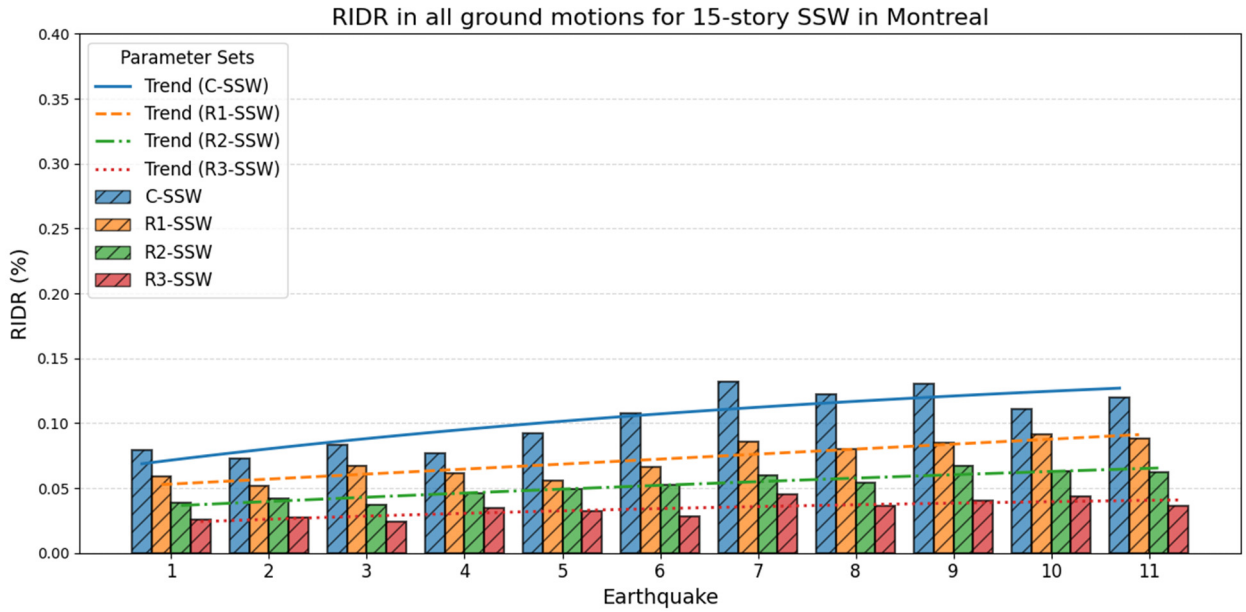

Figure 20. Reduction of RIDR in 15-story SSW located in Montreal, due to strengthening schemes, in all scenarios.

6.3. Shear Force Demand

In the case of ductile shear walls, it is essential for flexural failure to prevail as the primary mode of failure. Any flexural demand escalation may result in an elevated shear demand on the walls. Therefore, this study sought to assess potential alterations in shear force demands resulting from implementing strengthening schemes. Analyzing the mean base shear force demand for FRP-strengthened shear walls in response to ground motions revealed that, while the application of EB-FRP sheets has the potential to mitigate residual displacement and drift in these walls, it may also result in an increased demand for base shear in all seismic scenarios. The variations in shear force demand resulting from the implementation of the suggested strengthening strategies are depicted in Figures 21 and 22 for the shear walls in Vancouver and Montreal, respectively. To enhance comprehension, the shear force demands have been normalized against the base shear force demand in the control wall (C-SSW), and the vertical axis has been scaled relative to the height of the walls.

In line with earlier sections, separate illustrations depict the mean response envelopes for all scenarios. Notably, for walls situated in Vancouver, a conspicuous disparity emerges between the shear demand resulting from the M9 scenario and ground motions featuring higher frequency content. This observed phenomenon, where the base shear demand in the M9 scenario is lower than in the other scenarios, may be attributed to the plastic effects induced by higher vibration modes, a topic addressed in greater detail elsewhere [25]. Furthermore, this dissimilarity is accentuated in taller shear walls, underscoring the greater sensitivity of taller shear walls to higher modes. In the meantime, the findings have revealed that applying strengthening strategies leads to an increase in the base shear force requirements for SSWs. As an illustrative example, in the 20-story SSW located in Vancouver, namely R1-SSW, R2-SSW, and R3-SSW, the use of these methods resulted in an increase of respectively 4%, 6%, and 12% in the base shear demand. Similarly, for a 15-story shear wall, the increments were 8%, 11%, and 16%. The increase in shear demand due to the implementation of EB-FRP composites can be attributed to two key factors. Firstly, it arises from the confinement effect and flexural strengthening, which effectively enhances the post-yield stiffness in these structural elements. Secondly, adopting strengthening schemes reduces the structural vibration period, collectively leading to an amplified shear demand on the walls [3,11,47,55]. In Eastern Canada, the 20-story wall, denoted as R1-SSW, R2-SSW, and R3-SSW, experienced increases in base shear demand by 7%, 10%, and 14%,

respectively. Similarly, in its base shear demand, the 15-story SSW experienced increases up to 12%, 18%, and 23%. It is important to emphasize that the additional shear capacity due to horizontal EB-FRP exceeds the shear demand increase within the walls.

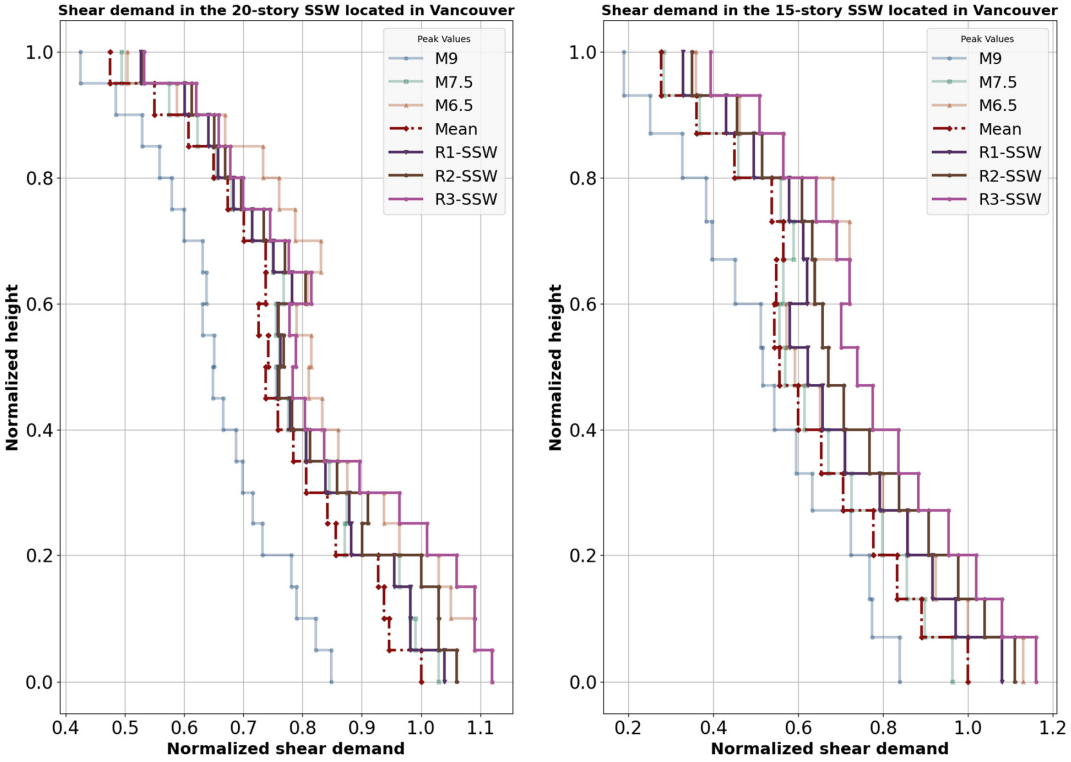

Figure 21. Shear demand in the 20-story and 15-story SSWs located in Vancouver due to different scenarios.

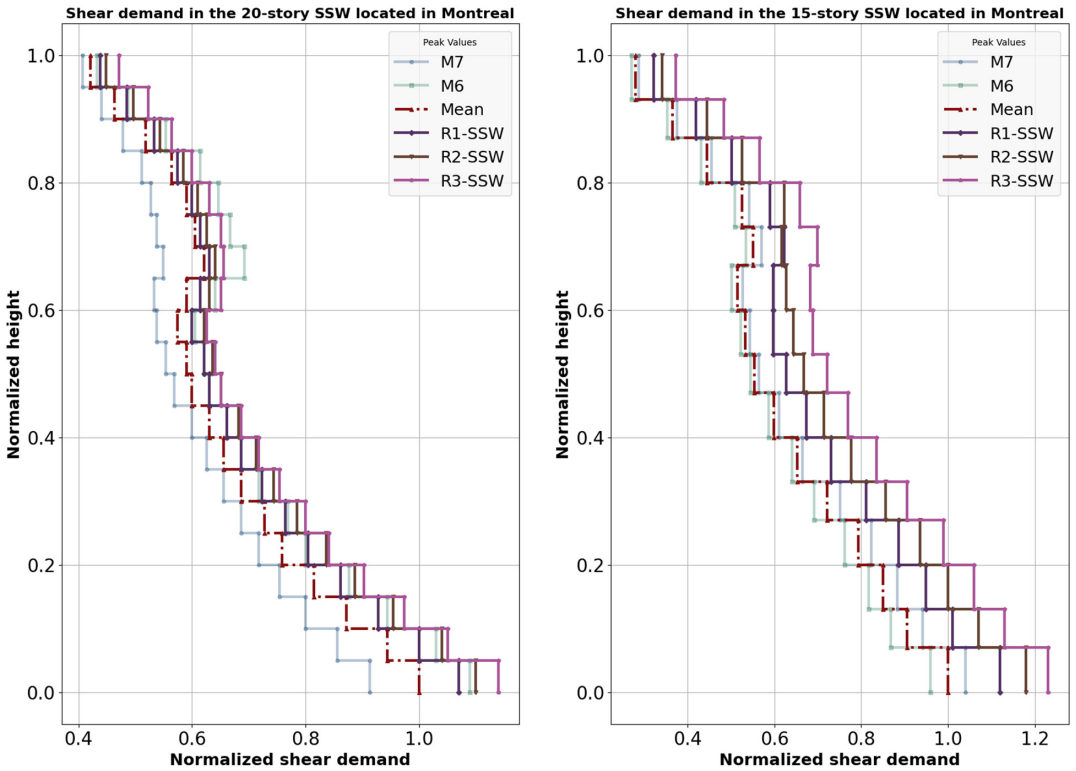

Figure 22. Shear demand in the 20-story SSWs located in Montreal due to different scenarios.

6.4. Bending Moment Demand

Despite the enhanced flexural capacity, the strengthening strategies amplified the bending moment demand in all specimens. In this context, the 15-story SSW located in Vancouver exhibited a 4% increase in bending moment demand at its base level under the R1-SSW scheme. On the other hand, the R2-SSW and R3-SSW configurations featured a 6% and 9% rise in bending moment demands for the same wall, respectively. As scenarios with higher frequency content (M6.5 and M7.5) were considered, the upper stories experienced more significant bending. In contrast, the lower stories bore the brunt of significant bending moments due to Cascadia events (M9). This phenomenon was more pronounced in taller walls, possibly attributable to the heightened influence of higher modes, which tend to be more pronounced in high-rise structures. Furthermore, when applying EB-FRP sheets, the 20-story wall demonstrated a relatively minor increase in bending moment demands. Under the R1-SSW, R2-SSW, and R3-SSW schemes, the wall experienced increases of 3%, 4%, and 7%, respectively.

In Eastern Canada, the influence of higher modes was more pronounced in the 20-story wall, particularly in the upper levels, where the disparity in bending moment demand caused by M6 and M7 was more conspicuous. However, the M7 scenario remained dominant in the lower levels in both shear walls. In Montreal, the 15-story wall with the R3-SSW strengthening scheme experienced the highest increase in base bending demand, recording an 11% rise. Comparatively, the increases in R2-SSW and R1-SSW were 6% and 4%, respectively. Additionally, in the case of the 20-story shear wall, there were increases of 9%, 6%, and 4% observed in R3-SSW, R2-SSW, and R1-SSW, respectively. Figures 23 and 24 show the variation in bending moment demand in shear walls located in Vancouver and Montreal, respectively. In these figures, bending moments are normalized with respect to base bending moment in C-SSW.

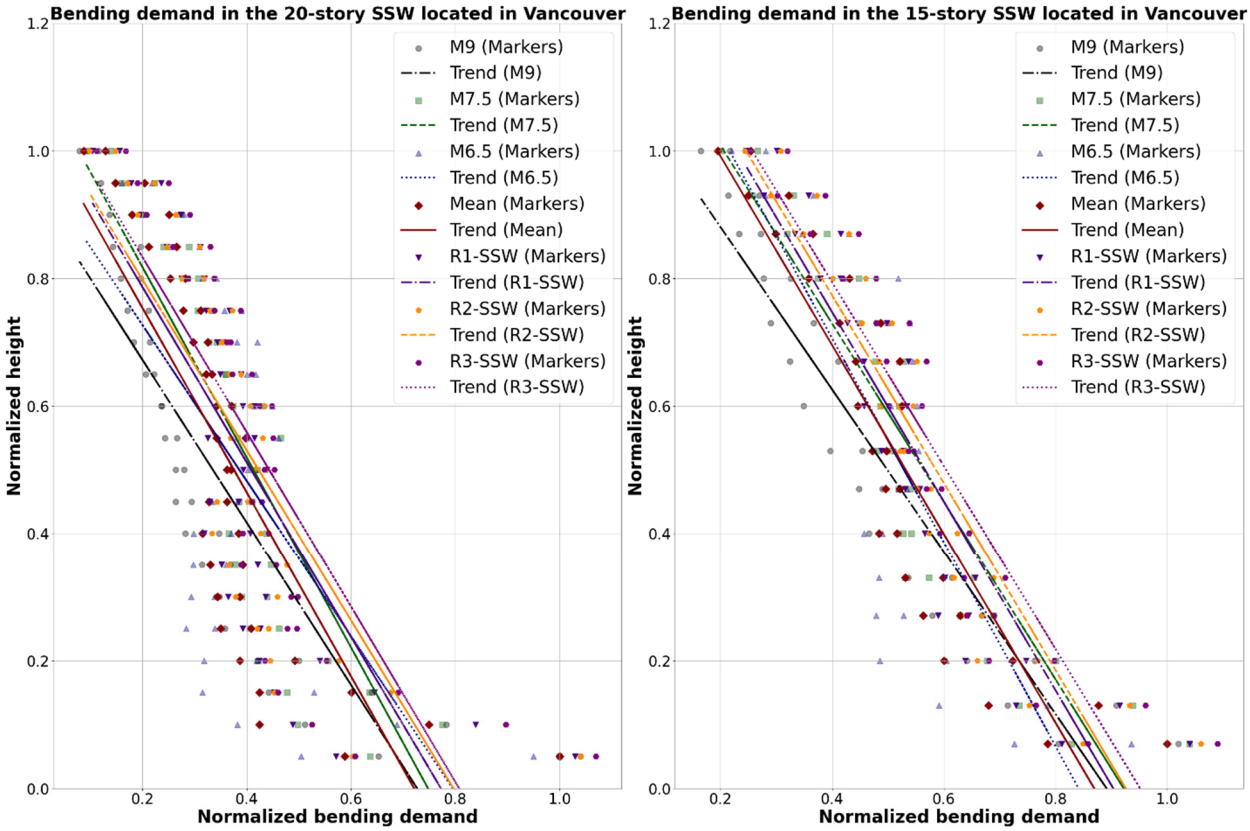

Figure 23. Bending demand in the 15-story SSWs located in Vancouver due to different scenarios.

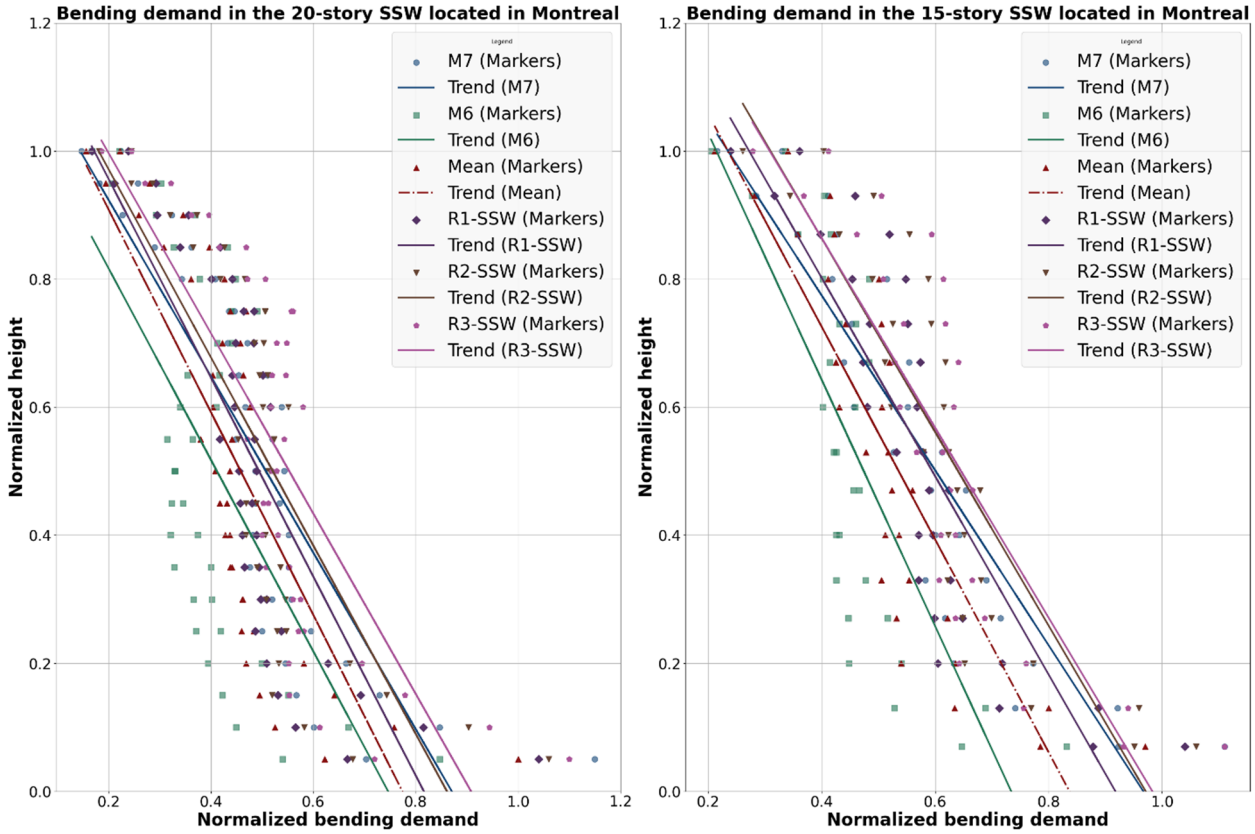

Figure 24. Bending demand in the 20-story SSWs located in Montreal due to different scenarios.

Although these increases did not exceed the shear and bending capacity of the shear walls in this study, excessive increases could pose problems. Therefore, it is crucial to check the force demand increase in buildings within the practical implications of the proposed method. Increased base shear demands can lead to higher stress levels in existing foundations and connections, potentially necessitating additional strengthening measures. Similarly, increased bending moments require careful consideration of the existing reinforcement to prevent failures. Strategic decision-making processes are essential to ensure that these increased demands do not compromise structural integrity or result in economic inefficiencies. Sherzer et al. [56] emphasized the need for a comprehensive assessment of safety and economic aspects in seismic retrofitting, highlighting the importance of balancing enhanced seismic performance with retrofitting cost.

Building owners must consider the cost of the proposed strengthening method. Decisions should be based on: 1—the cost of strengthening versus the benefit of enhanced resilience; if the main objective is to decrease residual displacement, this may take priority despite the costs; 2—the cost-effectiveness of the strengthening given the increased demands; and 3—the building's importance, determining how much investment is necessary and whether the proposed method satisfies the requirements. By integrating these considerations into strategic decision-making, we can achieve a balance between enhanced seismic resilience and maintaining safety and economic viability in existing structures.

7. Conclusions

The current investigation has assessed a novel approach for mitigating residual deformations in newly designed existing slender medium- to high-rise ductile shear walls. The primary technique employed to achieve this objective involved applying FRP sheets bonded to the shear wall surfaces. Within this investigation, four walls were designated as control specimens. These control specimens consisted of two 20-story and two 15-story walls, one of each located in Montreal and Vancouver, serving as representatives of the

Eastern and Western Canadian seismic zones. Three innovative strengthening configurations were devised for these walls, and their response to scaled ground motions was comprehensively assessed through two-dimensional nonlinear time history analysis. The following conclusions can be drawn:

1. The proposed configurations effectively reduced shear wall drift by a range of 8% to 28%, with the R3-SSW scheme featuring the highest performance level. However, the efficiency of EB-FRP sheets in SSWs diminishes as the wall height increases.
2. Cascadia subduction earthquakes, with a magnitude of M9, pose a unique challenge in Western Canada due to their low-frequency characteristics, which can excite the first vibration mode of SSWs and elevate flexural demands within the walls. Furthermore, their prolonged duration results in many loading and unloading cycles, ultimately leading to structural fatigue. Consequently, these seismic events influence the seismic behavior of shear walls in Vancouver, contributing to a substantial portion of the residual drift in western walls (1.42%).
3. The proposed strengthening schemes led to a significant reduction in RIDR (from 8% to 66%) within shear walls. Among the various configurations tested, R3-SSW emerged as the top performer. This outcome underscores the effectiveness of enhancing shear walls by bolstering the concrete compressive capacity, curbing crack propagation originating from substantial bending moments at the wall base, and mitigating concrete crushing in wall corners—a significant contributor to ductile slender wall failures. Furthermore, the use of vertical EB-FRP sheets at the extremities of the walls enhances flexural stiffness by harnessing their substantial tensile strength and limiting flexural cracks in the boundary elements of the walls.
4. Given the relatively low to medium intensity of ground motions experienced in Eastern Canada, these seismic events did not induce significant residual deformations in slender shear walls. Maximum permanent drift deformations observed are 0.13% in 15-story walls and less than 0.05% in 20-story walls. Particularly in taller shear walls within this region, the seismic response tends to remain predominantly elastic, suggesting that their strengthening may not be required.
5. The limited efficiency of R1-SSW and R2-SSW indicates that incorporating vertical EB-FRP sheets in the central portion of wall lengths is not as beneficial compared to the outer edges of the walls.
6. Using EB-FRP sheets increases base shear demand within the walls, ranging from 4% to 23%. In Western Canada, the shear demand is predominantly influenced by the scenarios of M7.5 and M6.5 due to the plastic effects of higher modes in SSWs. Additionally, as wall height increases, the impact of higher modes on base shear demand becomes more pronounced.
7. The additional shear capacity provided by horizontal EB-FRP exceeds the increased shear demand within the walls. However, while these methods enhance shear capacity beyond the increased demand, it is essential to evaluate their cost-effectiveness. The main objective of this study is to propose an effective method to reduce residual displacement in shear walls. It is crucial to consider the rationale behind this practice. The proposed method can be effective if the primary goal is to minimize residual displacement. However, if the objective is to reduce post-earthquake maintenance and repair costs, a cost-effectiveness analysis may be necessary to fully assess the benefits of the implemented strategies. Further discussion on this topic can be found elsewhere [57,58].
8. The proposed strengthening configurations elevate the bending moment demand within shear walls by 3% to 13%. As wall height increases, the influence of strengthening schemes on flexural demand tends to decrease.
9. Future research should focus on several key areas to optimize the use of FRP in seismic retrofitting. Exploring alternative materials that might offer similar benefits at reduced costs or improved performance could provide valuable insights. Additionally, investigating hybrid strengthening methods that combine FRP with other retrofitting

techniques could lead to innovations in seismic resilience strategies. Finally, long-term durability studies under cyclic loading conditions are crucial to understand the longevity and performance of FRP-strengthened structures over time.

10. The impact of ground motion characteristics on NLTH analysis has been found to be profound. Factors such as tectonic conditions, ground motion magnitudes, source-to-site distances, and soil type play critical roles. The frequency content and ground motion duration, shaped by these factors, dictate the structure's response to seismic waves. Consequently, cities with similar frequency content and ground motion durations to Montreal and Vancouver are expected to exhibit similar NLTH responses. However, further studies are required to evaluate the precise effects of other features of ground motions and tectonic conditions on the nonlinear response of buildings in cities with similar seismic activities.
11. The selected number of ground motions, while representative, may not encompass the full range of possible seismic events. The selection and scaling procedure, though consistent with NBCC guidelines, introduces another layer of approximation that can influence the accuracy of the nonlinear time history analysis. This becomes especially important when the study clearly demonstrates the impact of ground motion frequency content.
12. Future experimental studies are required to validate the numerical findings through real-world verification of the bonding behavior between EB-FRP composites and shear walls, accurately capture the hysteretic behavior under seismic loads, and confirm the overall performance and effectiveness of the strengthening schemes beyond modeling accuracy.

Author Contributions: Conceptualization, A.A. and O.C.; methodology, A.A. and O.C.; Literature review, A.A.; investigation, A.A. and O.C.; resources, O.C.; writing—original draft preparation, A.A.; writing—review and editing, O.C.; supervision, O.C.; project administration, O.C.; funding acquisition, O.C. All authors have read and agreed to the published version of the manuscript.

Funding: O.C. is funded by the National Science and Engineering Council (NERC) of Canada and by the Fonds de Recherche du Quebec–Nature et Technologie (FRQ-NT).

Data Availability Statement: The data supporting the finding of this study are available within the article.

Acknowledgments: The financial support of the Natural Sciences and Engineering Research Council of Canada (NSERC) and the Fonds de Recherche du Québec–Nature et Technologie (FRQ-NT) through operating grants is gratefully acknowledged.

Conflicts of Interest: The authors declare no conflict of interest.

References

1. National Building Code of Canada (NBCC). *Institute for Research in Construction*; National Research Council of Canada: Ottawa, ON, Canada, 2020.
2. Bruneau, M.; Reinhorn, A. Overview of the resilience concept. In Proceedings of the 8th US National Conference on Earthquake Engineering, San Francisco, CA, USA, 18–22 April 2022; pp. 18–22.
3. Abbaszadeh, A.; Chaallal, O. Resilience of medium-to-high-rise ductile coupled shear walls located in canadian seismic zones and strengthened with externally bonded fiber-reinforced polymer composite: Nonlinear time history assessment. *J. Compos. Sci.* **2023**, *7*, 317. [CrossRef]
4. Bedriñana, L.A.; Tani, M.; Kono, S.; Nishiyama, M. Evaluation of the Seismic Performance of Unbonded Post-Tensioned Precast Concrete Walls with Internal and External Dampers. II: Design Criteria and Numerical Research. *J. Struct. Eng.* **2022**, *148*, 04022106. [CrossRef]
5. Zhong, C.; Christopoulos, C. Self-centering seismic-resistant structures: Historical overview and state-of-the-art. *Earthq. Spectra* **2022**, *38*, 1321–1356. [CrossRef]
6. Naeem, A.; Kim, J. Seismic performance evaluation of a spring viscous damper cable system. *Eng. Struct.* **2018**, *176*, 455–467. [CrossRef]
7. Noureldin, M.; Memon, S.A.; Gharagoz, M.; Kim, J. Performance-based seismic retrofit of RC structures using concentric braced frames equipped with friction dampers and disc springs. *Eng. Struct.* **2021**, *243*, 112555. [CrossRef]

8. Fortunato, A.; Fabbrocino, F.; Angelillo, M.; Fraternali, F. Limit analysis of masonry structures with free discontinuities. *Meccanica* **2018**, *53*, 1793–1802. [CrossRef]
9. GangaRao, H.V.; Taly, N.; Vijay, P. *Reinforced Concrete Design with FRP Composites*; CRC Press: Boca Raton, FL, USA, 2006.
10. Deng, K.; Pan, P.; Shen, S.; Wang, H.; Feng, P. Experimental study of FRP-reinforced slotted RC shear walls under cyclic loading. *J. Compos. Constr.* **2018**, *22*, 04018017. [CrossRef]
11. El-Sokkary, H.; Galal, K.; Ghorbanirenani, I.; Léger, P.; Tremblay, R. Shake table tests on FRP-rehabilitated RC shear walls. *J. Compos. Constr.* **2013**, *17*, 79–90. [CrossRef]
12. Altin, S.; Anil, Ö.; Kopraman, Y.; Kara, M.E. Hysteretic behavior of RC shear walls strengthened with CFRP strips. *Compos. Part B Eng.* **2013**, *44*, 321–329. [CrossRef]
13. Huang, Z.; Shen, J.; Lin, H.; Song, X.; Yao, Y. Shear behavior of concrete shear walls with CFRP grids under lateral cyclic loading. *Eng. Struct.* **2020**, *211*, 110422. [CrossRef]
14. Sakr, M.A.; El-Khoriby, S.R.; Khalifa, T.M.; Nagib, M.T. Modeling of RC shear walls strengthened by FRP composites. *Struct. Eng. Mech.* **2017**, *61*, 407–417. [CrossRef]
15. Cruz-Noguez, C.A.; Lau, D.T.; Sherwood, E.G.; Hiotakis, S.; Lombard, J.; Foo, S.; Cheung, M. Seismic behavior of RC shear walls strengthened for in-plane bending using externally bonded FRP sheets. *J. Compos. Constr.* **2015**, *19*, 04014023. [CrossRef]
16. El-Sokkary, H.; Galal, K. Seismic behavior of RC shear walls strengthened with fiber-reinforced polymer. *J. Compos. Constr.* **2013**, *17*, 603–613. [CrossRef]
17. Khalil, A.; Ghobarah, A. Behaviour of rehabilitated structural walls. *J. Earthq. Eng.* **2005**, *9*, 371–391. [CrossRef]
18. El-Sokkary, H. Nonlinear behaviour of FRP-retrofitted RC coupled shear walls. *Structures* **2023**, *47*, 324–337. [CrossRef]
19. Shen, J.; Huang, Z.; Song, X.; Yao, Y. Deformation performance analysis of concrete shear wall with CFRP grids based on the modified uniaxial shear-flexural model. *J. Build. Eng.* **2022**, *54*, 104621. [CrossRef]
20. Song, X.; Huang, Z.; Shen, J.; Yao, Y. Experimental study on cyclic behavior of hybrid CFRP grids-steel shear walls. *Structures* **2020**, *28*, 496–511. [CrossRef]
21. Zhao, Q.; Zhao, J.; Dang, J.-T.; Chen, J.-W.; Shen, F.-Q. Experimental investigation of shear walls using carbon fiber reinforced polymer bars under cyclic lateral loading. *Eng. Struct.* **2019**, *191*, 82–91. [CrossRef]
22. *Standard CAN-A23.3-19*; Design of Concrete Structures for Buildings. Canadian Standards Association (CSA): Rexdale, ON, Canada, 2019.
23. Adebar, P.; Mutrie, J.G.; Devall, R.; Mitchell, D. Seismic Design of Concrete Shear Wall Buildings: New Requirements of CSA Standard a23. 3–2014. Available online: https://www.caee.ca/pdf/Paper_99063.pdf (accessed on 25 December 2023).
24. Cement Association of Canada. *Concrete Design Handbook*, 4th ed.; Cement Association of Canada: Ottawa, ON, Canada, 2016.
25. Adebar, P.; Dezhdar, E.; Yathon, J. Accounting for higher mode shear forces in concrete wall buildings: 2014 CSA A23. 3. In Proceedings of the 11th Canadian Conference on Earthquake Engineering, Quebec, QC, Canada, 17–20 June 2020.
26. Adebar, P.; Mutrie, J.; DeVall, R. Ductility of concrete walls: The Canadian seismic design provisions 1984 to 2004. *Can. J. Civ. Eng.* **2005**, *32*, 1124–1137. [CrossRef]
27. Bohl, A.G. Plastic Hinge Length in High-Rise Concrete Shear Walls. Ph.D. Thesis, University of British Columbia, Vancouver, BC, Canada, 2006.
28. *Analysis Reference Manual for SAP2000 Ultimate v. 21.0.2*; CSI: Berkeley, CA, USA, 2016.
29. National Research Council Canada. *Guide for the Design and Construction of Externally Bonded FRP Systems for Strengthening Concrete Structures (ACI 440.2 R-17)*; American Concrete Institute: Farmington Hills, MI, USA, 2017.
30. Ceroni, F.; Pecce, M.; Matthys, S.; Taerwe, L. Debonding strength and anchorage devices for reinforced concrete elements strengthened with FRP sheets. *Compos. Part B Eng.* **2008**, *39*, 429–441. [CrossRef]
31. Grelle, S.V.; Sneed, L.H. Review of anchorage systems for externally bonded FRP laminates. *Int. J. Concr. Struct. Mater.* **2013**, *7*, 17–33. [CrossRef]
32. Mostafa, A.; Razaqpur, A.G. CFRP anchor for preventing premature debonding of externally bonded FRP laminates from concrete. *J. Compos. Constr.* **2013**, *17*, 641–650. [CrossRef]
33. Carr, A. *RUAUMOKO, Computer Program Library*; Department of Civil Engineering, University of Canterbury: Christchurch, New Zealand, 2004.
34. NRCC. *Structural Commentaries (User's Guide—NBC 2015: Part 4 of Division B)*; National Research Council Canada (NRCC): Ottawa, ON, Canada, 2015.
35. Boivin, Y.; Paultre, P. Seismic performance of a 12-storey ductile concrete shear wall system designed according to the 2005 National building code of Canada and the 2004 Canadian Standard Association standard A23. 3. *Can. J. Civ. Eng.* **2010**, *37*, 1–16. [CrossRef]
36. Giberson, M.F. Two nonlinear beams with definitions of ductility. *J. Struct. Div.* **1969**, *95*, 137–157. [CrossRef]
37. Dezhdar, E. Seismic Response of Cantilever Shear Wall Buildings. Ph.D. Thesis, University of British Columbia, Vancouver, BC, Canada, 2012.
38. Honarparast, S.; Chaallal, O. Non-linear time history analysis of reinforced concrete coupled shear walls: Comparison of old design, modern design and retrofitted with externally bonded CFRP composites. *Eng. Struct.* **2019**, *185*, 353–365. [CrossRef]
39. Imbsen Software Systems. *XTRACT—Cross-Sectional X sTRuctural Analysis of ComponenTs v2.6.0*; Imbsen Software Systems: Lowell, MA, USA, 2004.

40. Mander, J.B.; Priestley, M.J.; Park, R. Theoretical stress-strain model for confined concrete. *J. Struct. Eng.* **1988**, *114*, 1804–1826. [CrossRef]
41. Lam, L.; Teng, J.G. Design-oriented stress–strain model for FRP-confined concrete. *Constr. Build. Mater.* **2003**, *17*, 471–489. [CrossRef]
42. Sherzer, G.L.; Alghalandis, Y.F.; Peterson, K. Introducing fracturing through aggregates in LDPM. *Eng. Fract. Mech.* **2022**, *261*, 108228. [CrossRef]
43. McNeice, D. Performance-Based Design of a 30-Storey Coupled Wall Structure. Master's Thesis, University of South Carolina, Columbia, SC, USA, 2004.
44. Li, Z. Seismic Vulnerability of RC Frame and Shear Wall Structures in Singapore. 2006. Available online: https://core.ac.uk/download/pdf/48645958.pdf (accessed on 25 December 2023).
45. Saiidi, M.; Sozen, M.A. *Simple and Complex Models for Nonlinear Seismic Response of Reinforced Concrete Structures*; University of Illinois Engineering Experiment Station. College of Engineering: Champaign, IL, USA, 1979.
46. Hall, J.F. Problems encountered from the use (or misuse) of Rayleigh damping. *Earthq. Eng. Struct. Dyn.* **2006**, *35*, 525–545. [CrossRef]
47. Honarparast, S.; Chaallal, O. Seismic performance of coupled shear walls designed according to old and new codes and retrofitted with Eb-CFRP composites. *J. Earthq. Eng.* **2022**, *26*, 1875–1898. [CrossRef]
48. Adams, J.; Allen, T.; Halchuk, S.; Kolaj, M. Canada's 6th Generation Seismic Hazard Model, as Prepared for the 2020 National Building Code of Canada. In Proceedings of the 12th Canadian Conference on Earthquake Engineering, Quebec, QC, Canada, 17–20 June 2019.
49. Tremblay, R.; Atkinson, G.M. Comparative study of the inelastic seismic demand of eastern and western Canadian sites. *Earthq. Spectra* **2001**, *17*, 333–358. [CrossRef]
50. Atkinson, G.M. Earthquake time histories compatible with the 2005 National building code of Canada uniform hazard spectrum. *Can. J. Civ. Eng.* **2009**, *36*, 991–1000. [CrossRef]
51. Adams, J.; Atkinson, G. Development of seismic hazard maps for the proposed 2005 edition of the National Building Code of Canada. *Can. J. Civ. Eng.* **2003**, *30*, 255–271. [CrossRef]
52. Tremblay, R.; Atkinson, G.M.; Bouaanani, N.; Daneshvar, P.; Léger, P.; Koboevic, S. Selection and scaling of ground motion time histories for seismic analysis using NBCC 2015. In Proceedings of the 11th Canadian Conference on Earthquake Engineering (11CCEE), Victoria, BC, Canada, 21–24 July 2015; p. 69.
53. ASCE. *Minimum Design Loads and Associated Criteria for Buildingsand other Structures*; ASCE/SEI 7-22; ASCE: Reston, VA, USA, 2022.
54. Arabzadeh, H.; Galal, K. Effectiveness of FRP wraps for retrofitting of existing RC shear walls. In Proceedings of the 11th Canadian Conference on Earthquake Engineering, Victoria, BC, Canada, 21–24 July; pp. 21–24.
55. Arabzadeh, H.; Galal, K. Seismic collapse risk assessment and FRP retrofitting of RC coupled C-shaped core walls using the FEMA P695 methodology. *J. Struct. Eng.* **2017**, *143*, 04017096. [CrossRef]
56. Lifshitz Sherzer, G.; Urlainis, A.; Moyal, S.; Shohet, I.M. Seismic Resilience in Critical Infrastructures: A Power Station Preparedness Case Study. *Appl. Sci.* **2024**, *14*, 3835. [CrossRef]
57. Egbelakin, T.; Wilkinson, S. Factors affecting motivation for improved seismic retrofit implementation. In Proceedings of the Australian Earthquake Engineering Conference (AEES), Adelaide, Australia, 21–23 November 2008.
58. Egbelakin, T.; Wilkinson, S.; Ingham, J. Economic impediments to successful seismic retrofitting decisions. *Struct. Surv.* **2014**, *32*, 449–466. [CrossRef]